Spring 2018

Temperature and Electric Field Dependency of Asymmetric Stretching of Nitrate and Carbonate Ions

Konnor Jones
Western Kentucky University, konnor.jones391@topper.wku.edu

ENERGETIC STABILITY OF NITRATE AND CARBONATE ION SOLVATION GEOMETRIES IN SOLUTION

A Thesis
Presented to
The Faculty of the Department of Chemistry
Western Kentucky University
Bowling Green, Kentucky

In Partial Fulfillment
Of the Requirements for the Degree
Master of Science

By
Konnor Jones

May 2018

ENERGETIC STABILITY OF NITRATE AND CARBONATE ION SOLVATION GEOMETRIES IN SOLUTION

Date Recommended 4/4/18

Matthew Nee 4/4/2018
Dr. Matthew Nee, Director of Thesis

Jeremy Maddox
Dr. Jeremy Maddox

Eric Conte
Dr. Eric Conte

T. Scott
Dean, Graduate Studies and Research

4/9/18
Date

ACKNOWLEGEMENTS

I would like to thank my advisor, Dr. Matthew Nee for all of the support and guidance that he has provided to me throughout my time at Western Kentucky University (WKU). I strongly believe that if he was not my advisor that I would not be the scientist that I am today.

Another person who has greatly helped me throughout my college career is my High School English teacher, Ms. Natalie Croney. Without the advice that she gave me, I believe that I would have been unable to pursue a Masters in Chemistry.

As I encountered multiple obstacles in my research, I have always been able to ask Mrs. Alicia Pesterfield for assistance. If it was not for her help, my research projects would have been significantly delayed, preventing me from obtaining the progress that I have achieved in my research.

Thank you to my friends (especially Drake Ballentine, Jesús Berlanga, and Melanie Couch) and parents (Ken and Rachel Jones) for all of the help that you have provided inside and outside of my school work. Without the support from these people, I would not be able reach this point in my education.

This work was funded by a WKU internal grant (FUSE 16-FA238) and the WKU Research and Creative Activities Program (RCAP 16-8003). Kentucky Space Grant Consortium (KSGC 3048107645-13-146)

CONTENTS

LIST OF FIGURES

LIST OF TABLES

ENERGETIC STABILITY OF NITRATE AND CARBONATE ION SOLVATION GEOMETRIES IN SOLUTION

Konnor Jones May 2018 70 Pages

Directed by: Dr. Matthew Nee, Dr. Jeremy Maddox, and Dr. Eric Conte

Department of Chemistry Western Kentucky University

Photolysis of nitrate ion in the natural environment produces NO, NO_2, and O_3, releasing these toxic gases into the atmosphere. Work done by other groups has shown ionic strength dependence of the ratio of products from photolysis of aqueous nitrate ion. To better understand the kinetic mechanisms of nitrate photolysis, the effects that ionic strength in solution have on nitrate ion symmetry breaking are needed. Different solvation environments induce nitrate bonding motifs that may be correlated to the product ratio. Fourier-transform infrared spectra of aqueous nitrate–ion solutions were obtained over a range of temperatures for several total electrolyte concentrations. The electric fields (arising from water molecules and ions in solution) in aqueous potassium nitrate solution distort the trigonal planar shape of the nitrate ion, which may favor a specific initial path of the decomposition of nitrate during photolysis. Van't Hoff plots of the relative peak areas corresponding to the formally-degenerate asymmetric stretching mode reveal the relative energies of the two solvation geometries. The difference in energy between the two geometries is linearly proportional to the ionic strength of the solution. Electronic structure calculations suggest that the more symmetric geometry has an increased stability relative to the less-symmetric geometry in high ionic strength solutions. Thus, the relative amounts of the nitrate ion solvation geometries can be correlated to the amount of products produced during photolysis to help explain the ionic-strength dependence of the product yields. Nitrate geometries at the water—CCl_4 interface and aqueous carbonate ion bonding motifs

are being investigated to identify pure-water effects. Preliminary results suggest that the more symmetric geometry nitrate is stabilized at the water—CCl_4 interface and the less-symmetric carbonate solvation geometry has an increased stability relative to the more symmetric geometry in high ionic strength solutions

1. Introduction

Nitrate and carbonate ions are ubiquitous in the natural environment and play a significant role in biological systems, organic synthesis, and environmental processes.[1–4] Both ions are vital for the health of living organisms. In agriculture, nitrate-based fertilizers are commonly used to promote crop growth. Many marine creatures have shells and exoskeletons that are composed of $CaCO_3$. The properties of the nitrate and carbonate ions must be studied to understand how the concentration of both ions change under dynamic environmental conditions and the extent to which these ions influence the environment.

1.1 Environmental Relevance

Both nitrate and carbonate ions are primary components in aerosols[5,6] and nitrate is prevalent in snowpack.[7] Aerosols affect the climate and temperature of the earth by altering the amount of thermal energy that is reflected and absorbed by the earth, which is known as radiative forcing.[8] The magnitude of the impacts these particles have on the global temperature is inconsistent between different atmospheric models; despite the ubiquity of aerosols, little is known about how the composition of the particles change as they age.[8–10] Because the optical properties of aerosols are dependent on the composition, the molecules that comprise these particles must be known to determine the extent that they contribute to the radiative forcing of the earth. Compositional changes of an aerosol are partially dictated by the molecules that reside at the surface of the particle.[9] Therefore, the radiative forcing characteristics of nitrate- and carbonate-containing aerosols is partly dependent on the location of the ions in the particle. The nitrate ion has been shown to preferentially reside at the air-water interface of bulk samples.[11,12] However, the planar air-water interface of bulk solutions is not an accurate representation of the aerosol surface because the curvature

of the particle alters the surface tension, requiring a spherical air-water interface to be investigated. Because the gas phase of the air-water interface is commonly described as a hydrophobic phase,[13] aqueous clusters that are dispersed in a hydrophobic solvent may be an accurate model of an aqueous aerosol. The location of ions in these clusters may be used to predict the location of the ions in aerosol particles.

Nitrate-containing aerosols that are suspended in the atmosphere are continuously deposited in snowpack, creating a distribution of nitrate in the snowpack.[14,15] The amount of nitrate that is deposited in the snowpack is consistent with the nitrate concentration in the atmosphere.[16] Buried in this chemically inert environment, the ion lies dormant in the medium where it acts as a record for the concentration of nitrate in the atmosphere at the time the ion was deposited.[15–19] Analysis of the vertical distribution of nitrate ion in snowpack enables the atmospheric nitrate concentration to be determined with respect to time. As the ions that lie dormant in the snowpack age, they decay radioactively with time to form isotopes.[18,20] Because the extent to which the nitrate ions decay radioactively is dependent on the age of the ions, the isotopes in the nitrate ions can be used to determine the approximate time the nitrate ions were deposited in the snowpack. This gives a record of the nitrate concentration during previous eras of the life of the earth, enabling previous atmospheric conditions to be determined. However, analysis of the nitrate ions in snowpack records is hindered through post-depositional processes.[16–18,21] Chemical processes such as photolysis significantly alter the concentration of nitrate in snowpack. To accurately interpret the nitrate concentration in snow records, the post-depositional processes that alter the nitrate concentration must be characterized.

1.2 Photolysis of Nitrate Ion

When snowpack is irradiated with ultraviolet (UV) radiation, the nitrate ion photodecomposes (according to the reaction mechanisms in Table 1.1) to produce NO_x ($NO + NO_2$), HO_x ($OH + HO_2$), and O_3.[3] These products are hazardous to living organisms and are released into the troposphere, where they react with other molecules to alter the composition of the atmosphere.[18] Of the photoproducts produced, HO_x and O_3 influence the oxidative capacity of the atmosphere by altering the lifetime of atmospheric pollutants and greenhouse gases. Since the photolysis of nitrate in snowpack significantly alters the concentrations of NO_x, HO_x, and O_3 in the atmosphere, the factors that influence the product ratio from the photolysis of nitrate need to be identified to model compositional changes of the atmosphere. This task is complicated by the two initial reaction pathways (reactions 1 and 2 in Table 1.1) that produce different products.[22] Because reactions are dependent on the products from preceding reactions, the product ratio from these two reactions dictate the amounts of NO_x, HO_x, and O_3 that are produced from the photolysis of the nitrate ion.

Two initial reaction pathways exist because the additional electron associates with the NO_2 moiety or the oxygen atom.[23] It is hypothesized here that the two pathways result from different nitrate ion solvation geometries that experience different kinetics. Identifying the solvation geometry and ionic strength effects on the photolysis kinetics of the nitrate ion may provide a molecular understanding of the work done by Grassian and coworkers who showed the amount of nitrite that is produced from the photolysis of aqueous nitrate is dependent on the concentration of nitrate in solution.[3] A molecular understanding of this work would allow the nitrate concentration dependence on the product ratio from the photolysis of the nitrate to be incorporated into atmospheric models.

Table 1.1 Reactions and rate constants in snow photochemistry models. Adapted from Ref. 22.

No.	Reaction	Reaction Rate Coefficient	Reference
1	NO_3^- $(+H^+) \xrightarrow{h\nu} NO_2 + OH$	1.3 x 10^{-5} s^{-1}	Ref. 22
2	$NO_3^- \xrightarrow{h\nu} NO_2^- + O(^3P)$	1.3 x 10^{-4} s^{-1}	Ref. 22
3	$NO_3^- + O(^3P) \rightarrow NO_2^- + O_2$	2.0 x 10^8 M^{-1} s^{-1}	Ref. 24
4	NO_2^- $(+H^+) \xrightarrow{h\nu} NO + OH$	1.5 x 10^{-3} M^{-1} s^{-1}	Ref. 21
5	$NO_2^- + OH \rightarrow NO_2 + {}^-OH$	1.0 x 10^{10} M^{-1} s^{-1}	Ref. 25
6	$NO_2 \xrightarrow{h\nu} NO + O(^3P)$	1 s^{-1}	Ref. 22
7	$2NO_2$ $(+H_2O) \rightarrow NO_3^- + NO_2^- + 2H^+$	1.0 x 10^7 M^{-1} s^{-1}	Ref. 26
8	$NO_2 + NO$ $(+H_2O) \rightarrow 2NO_2^- + 2H^+$	3.0 x 10^8 M^{-1} s^{-1}	Ref. 22
9	$NO_2 + OH \rightarrow NO_3^- + H^+$	5.0 x 10^9 M^{-1} s^{-1}	Ref. 22
10	$NO_2 \rightarrow NO_{2\ gas}$	41 s^{-1}	Ref. 19
11	$2NO$ $(+O_2) \rightarrow 2NO_2$	360 M^{-1} s^{-1}	Ref. 22
12	$NO + OH \rightarrow NO_2^- + H^+$	2.0 x 10^{10} M^{-1} s^{-1}	Ref. 22
13	$NO \rightarrow NO_{gas}$	410 s^{-1}	Ref. 19
14	$O(^3P)$ $(+O_2) \rightarrow O_3$	1.2 x 10^6 M^{-1} s^{-1}	Ref. 22
15	$NO_2^- + O(^3P) \rightarrow NO_3^-$	3.0 x 10 M^{-1} s^{-1}	Ref. 27
16	$NO_2^- + O_3 \rightarrow NO_3^- + O_2$	3.7 x 10^{-4} s^{-1}	Ref. 28
17	$H_2O_2 \xrightarrow{h\nu} 2OH$	1.18 x 10^{-4} s^{-1}	Ref.29,30
18	$H_2O_2 + OH \rightarrow HO_2 + H_2O$	8.0 x 10^6 M^{-1} s^{-1}	Ref. 31
19	$2HO_2 \rightarrow H_2O_2 + O_2$	1.4 x 10^5 M^{-1} s^{-1}	Ref. 32,33
20	$HO_2 + OH \rightarrow H_2O + O_2$	1.0 x 10^{10} M^{-1} s^{-1}	Ref. 34
21	$CH_2(OH)_2 + OH \rightarrow HO_2 + HCOOH + H_2O$	4.5 x 10^8 M^{-1} s^{-1}	Ref. 35

photolysis of the nitrate to be incorporated into atmospheric models.

1.3 Electronic Structure

The delocalized π-orbital that extends over the entire nitrate and carbonate ions causes the ions to be polarizable, making the trigonal planar geometry (D_{3h} symmetry) of the ions that is observed in the gas phase susceptible to changes from hydrogen bonding (H-bonding) and external electric fields.[36] This gas-phase symmetry causes the two asymmetric stretches of the nitrate ion in Figure 1.1 to be degenerate, which manifest as a single peak in the infrared (IR) spectrum. When the ions are introduced into an aqueous

environment, the D_{3h} symmetry is broken, lifting the degeneracy of the two asymmetric stretches of the ion. This manifest as a splitting of the asymmetric-stretch peak in the IR spectrum into two distinguishable peaks.

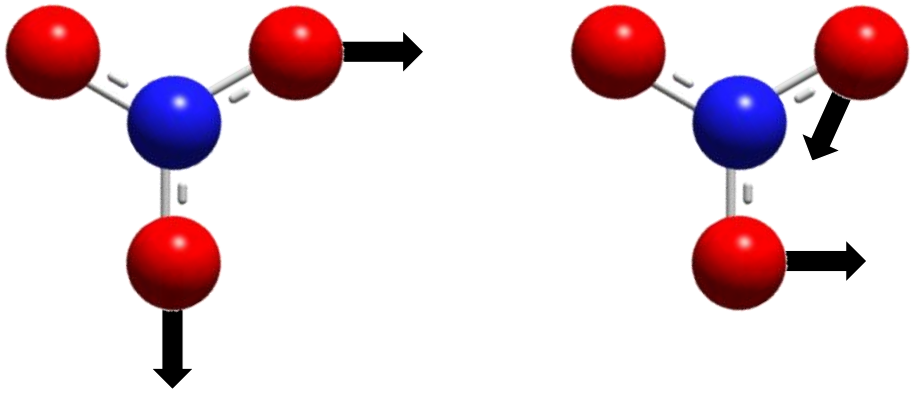

Figure 1.1. Asymmetric stretches of nitrate ion.

1.4 Solvation Structure

Grassian and coworkers[6] showed that the splitting of the two nitrate asymmetric-stretch features in the nitrate IR spectrum is proportional to the nitrate concentration in solution. Infrared multiple photon photodissociation (IRMPD) experiments conducted by Neumark and coworkers[36] showed the symmetry of the nitrate ion is broken upon the addition of a single water molecule to the nitrate ion. The immediate peak splitting when the nitrate ion is hydrated by a single water molecule suggests that the singly hydrated nitrate ion may be a valid model for the solvation geometry of the ion. Moreover, multidimensional spectra suggest that nitrate is actively engaged with a single water at a time, supporting the singly hydrated nitrate solvation model.[23] In the gas phase, the addition of multiple hydrating water molecules to the nitrate ion induces a larger splitting of the two

asymmetric-stretch features in the IR spectrum, suggesting that the magnitude of the peak splitting may be representative of the number of hydrating water molecules.[36] Because the carbonate ion also has a D_{3h} symmetry and experiences a breaking of symmetry when it is placed in an aqueous environment, it may be appropriate to expect carbonate to behave similarly to the nitrate ion in solution.

Multiple studies have searched for minimum energy structures for the nitrate ion that is hydrated by a varying numbers of water molecules.[37–39] Consistently, two minimum energy structures for the nitrate ion that is hydrated by a single water molecule have been found. As shown in Figure 1.2, the water molecule is singly- (C_s) or doubly- (C_{2v}) bound to the nitrate ion. The presence of two isosbestic points in UV absorption spectra of aqueous nitrate solutions supports the view that a chemical equilibrium between two nitrate structures exist in solution.[40]

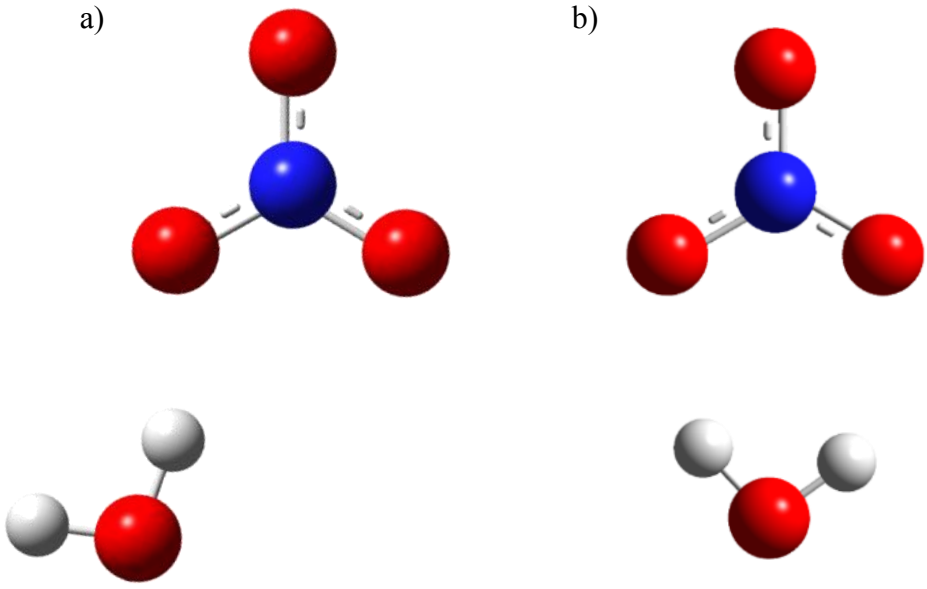

Figure 1.2. Optimized structures of singly- (a) and doubly- (b) bound solvation geometries of the nitrate ion.

1.5 Clusters Experiments

To obtain a molecular understanding of the solvation of ions in the bulk solution, the interactions between ions and hydrating water molecules must be understood. Because conventional spectroscopic methods (such as FTIR spectroscopy) probe the surface and the bulk phase of samples, molecules that are located in various solvation environments are interrogated, making it difficult to elucidate the molecular interactions between solute and solvent molecules. The interactions between a finite number of water molecules and an ion needs to be probed to understand solvation of ions in the bulk phase. The ability to produce microhydrated ions in the gas phase has made it possible to interrogate the interactions between an ion and a finite number of water molecules. In gas-phase cluster experiments, ions that are hydrated by a limited number of water molecules are produced and spectroscopically probed. Two common methods that are used to produce these clusters is the jet expansion or electrospray ionization of a fluid. Both techniques create clusters with a distribution of sizes.[36,41] The ability to mass select clusters allows ions with an incrementally increasing number of hydrating water molecules to be interrogated, facilitating the investigation of the hydration shell of ions. The low number density of the clusters that are produced during gas-phase experiments is below the sensitivity of conventional IR absorption measurements, requiring other methods, such as IRMPD spectroscopy, to be used because of its high sensitivity.[42] The primary drawback of the experiments that use these alternative techniques is that the instrumentation that is required to create and probe the clusters is financially expensive and technically difficult to use. To alleviate the difficulty of conducting gas-phase cluster experiments while still being able to probe the interactions between solute and solvent molecules, an alternative method that

disperses water in CCl_4 to create clusters of water was developed.

Dispersion of an electrolyte solution in CCl_4 is known to cause a portion of the ions to transfer from the aqueous phase into the hydrophobic phase. The ions that reside in the hydrophobic phase are hydrated by more than one water molecule. Unlike gas-phase experiments, in which a mass spectrometer is used to determine the composition of the cluster, mass spectrometry cannot be used to determine the size of the water clusters that are dispersed in CCl_4, preventing the composition of the water clusters to be accurately known. Therefore, the pure solute-water interactions cannot be definitively identified nor be correlated with bulk phase interactions. Changes to the water peaks that are present in the CCl_4 IR spectrum can be used to estimate the size and composition of water clusters that are dispersed in CCl_4. The presence of the broad water peak in the 2800—3600 cm^{-1} region indicates the presence of a hydrogen-bonding network, which is not observed in the FTIR water cluster spectrum. This water peak is absent in the IR spectrum of aqueous nitric acid clusters that are dispersed in CCl_4, indicating the nitric acid molecules are not solvated in large water clusters. Alterations to the nitric acid peaks in the IR spectrum indicate that the molecules are hydrated by no more than three water molecules. These results suggest that the water clusters that are created by the dispersion of water in a hydrophobic solvent are composed of approximately three water molecules or less. Even though these results suggest that the location of ions in aerosol size water clusters may not be identified from these experiments, the relative stability of the nitrate and carbonate ion solvation geometries in solution may be determined.

2. Experimental

FTIR spectroscopy was used to interrogate bulk and aqueous KNO_3 clusters while only bulk K_2CO_3 solutions were studied.

2.1 Reagents

Reagents that were used included KNO_3 (Aldrich, ≥ 99.0%), K_2CO_3 (Fischer, Certified ACS), NaCl (Aldrich, ≥ 99.5%), and CCl_4 (Aldrich, 99.9%). All reagents for the carbonate and aqueous KNO_3 cluster experiments were dried in an oven while only some of the KNO_3 and NaCl reagents that were used for the bulk phase nitrate experiments were dried. No differences were observed between the FTIR spectra of samples that were prepared with KNO_3 that was and was not dried in an oven. Molecular sieve was used to remove the water from the carbon tetrachloride. Absence of the water peaks from 2800—4000 cm^{-1} in the CCl_4 IR spectrum indicates the water concentration in the solvent is less than 73 μM.[43]

2.2 Sample Preparation

Aqueous 0.1 M KNO_3 and K_2CO_3 samples were prepared by dissolving 0.1011 g of KNO_3 or 0.1382 g of K_2CO_3 in 10 ml of deionized (18 MΩ) water. Sodium chloride was added to alter the ionic strength of the samples. Aliquots of the samples were placed on the center of a CaF_2 window. A 50-μm Teflon spacer and a second CaF_2 window were placed on top of the sample to create a thin layer of solution between the two windows. The assembly was then secured in the custom-built cell that is described in section 2.3.

Saturated KNO_3 solutions we prepared by dissolving KNO_3 until the crystals ceased to dissolve. Because water has a low solubility in CCl_4, aqueous KNO_3 was added to CCl_4 so the solution that is dispersed in the solvent may aggregate to form clusters. To control the

concentration of water in the aqueous KNO_3 cluster samples, all reagents were transferred in a nitrogen gas filled glove box (Vacuum Atmosphere Company) that was maintained at a 0% relative humidity (RH). Glassware that was used to prepare the cluster samples was placed under a vacuum of -20 in Hg in a glove box antechamber for three 5-min cycles to remove water that had adhered to the glass surface. In the glove box, the mouths of empty serum bottles were covered with multiple layers of Parafilm to act as a temporary septum, which can be easily pierced by large gauge needles. In an ambient atmosphere, an aliquot of an aqueous KNO_3 solution was extracted with a 10 μL glass syringe and weighed. The aliquot was transferred to the bottle by piercing the Parafilm septum and injecting the sample into the bottle. Immediately after the sample was transferred to the bottle, the puncture hole in the Parafilm was covered with additional layers of Parafilm to regulate the water concentration in the bottle. In the glove box, the Parafilm was replaced with a rubber stopper and a vial crimp seal. In the nitrogen atmosphere, dry CCl_4 was volumetrically measured and transferred to the septum capped bottle to maintain the water concentration in the sample. The sample was sonicated for 15 minutes to disperse aqueous KNO_3 clusters in the CCl_4. Without dispersion of the aqueous KNO_3, the multiple nitrate ions are more likely to reside in the same water cluster, resulting in nitrate-nitrate interactions. Because of the low number density of the clusters in the CCl_4, the sample was transferred to a long-path cell for the collection of spectra. Compared to the gas-phase clusters, the number density of the clusters that are dispersed in CCl_4 is significantly increased, enabling FTIR spectroscopy to be used.[43]

2.3 Instrumentation

To obtain information about the structure of the two nitrate and two carbonate species that are present in solution, a PerkinElmer Spectrum One Fourier-transform infrared (FTIR) spectrometer was used to collect spectra of bulk aqueous KNO_3 and K_2CO_3 solutions. Bulk liquid samples were contained between two CaF_2 windows that were separated by a 50-µm Teflon spacer. Calcium fluoride windows were used for all experiments because they are insoluble in water and they are transparent in the region of the IR spectrum that is of interest, as shown in Figure 2.1. An attempt was made to use Ge windows to collect spectra for the cluster experiment.

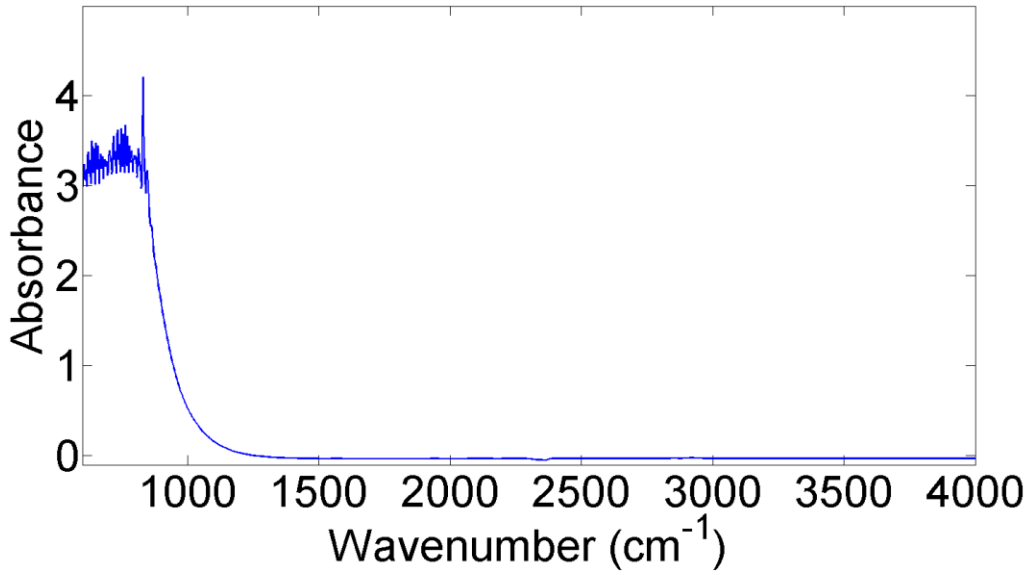

Figure 2.1. FTIR spectrum of CaF_2 windows.

For the bulk phase experiments, the IR windows were contained in a custom-built aluminum sample cell with a brass ring to secure the windows, which is shown in Figure 2.2. Aluminum and brass were chosen so the ring that secures the windows in the cell can be easily screwed in and out of the cell. Temperature-dependent spectra were obtained with

a Pike Technologies Falcon Mid-Infrared Transmission temperature controller. A Zalman Reserator1 V2 fanless water cooling system was used to maintain the temperature of the accessory. The concentration of water in low nitrate concentration samples was controlled by preparing the samples in a glove box. Samples were sonicated with a VWR ultrasonic cleaner.

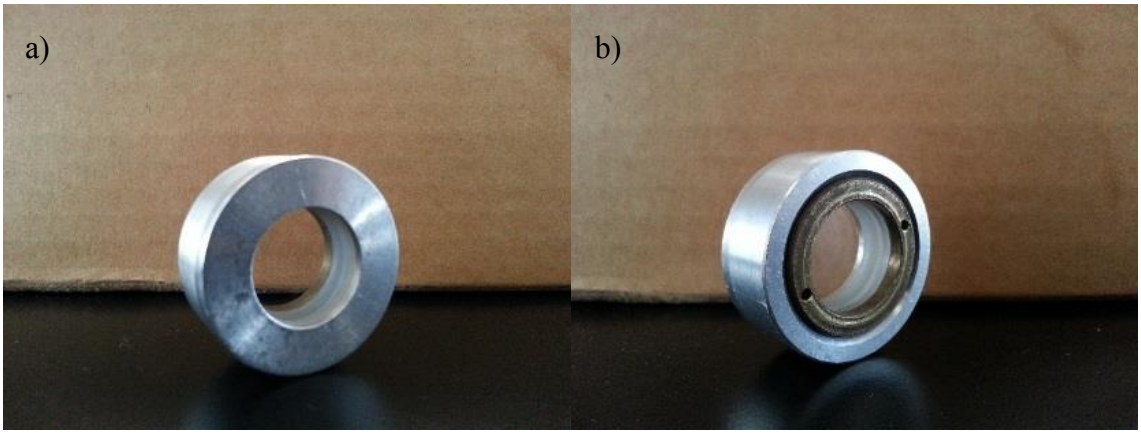

Figure 2.2. Front (a) and back (b) view of the custom-built sample cell that is used for bulk phase experiments.

2.4 Silanization of Glassware

To prevent water clusters from H-bonding to the glass long-path cell shown in Figure 2.3, the cell was silanized. The glass silanization procedure that was developed by Shultz and coworkers[43] was used and is briefly described. The glassware is cleaned with concentrated sulfuric acid and placed in DI water overnight to leach out residual acid. The glassware is soaked overnight in a 10% (v/v) dimethylethoxysilane and ethanol solution. Acetic acid is used to adjust the pH of the solution from 4.5-5.5. The silanol coating is heat

cured in a 110 °C oven for 10 minutes. Successful silanization of the glassware was identified by the beading of water on the glass surface as it is displayed in Figure 2.4.

Figure 2.3. Glass long-path cell with CaF_2 windows.

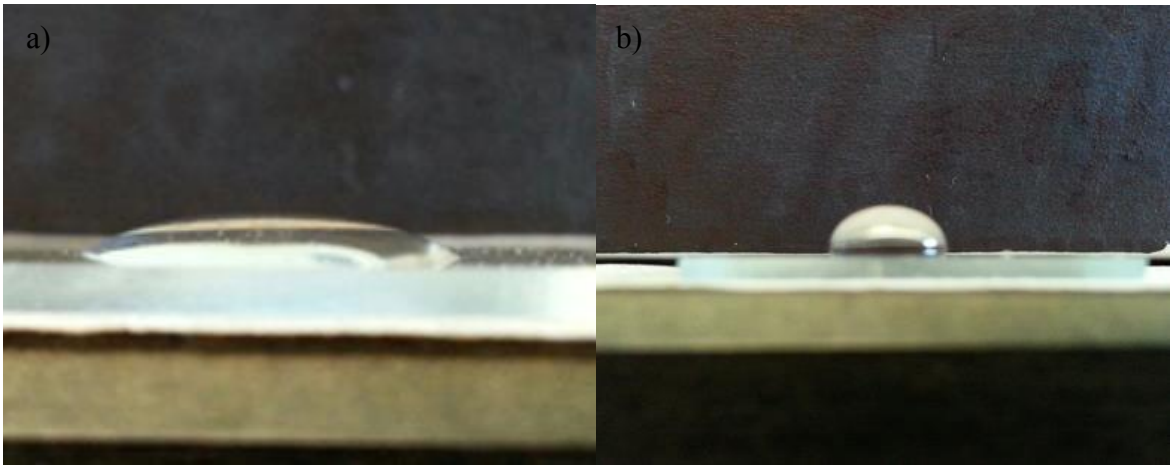

Figure 2.4. Water drop on a glass microscope slide before (a) and after (b) silanization.

2.5 Collection of FTIR spectra

For bulk phase experiments, a spectrum of 25 ˚C DI water was used as the background. Solutions were prepared the day the spectra were collected. Samples were warmed from 10 ˚C to 50 ˚C in 5 ˚C increments, with spectra collected at each temperature. To prevent condensation from forming on the windows, both CaF_2 windows were exposed to a constant stream of dry N_2 gas for temperatures below 25 ˚C. For each temperature that spectra were collected, the samples were allowed to thermally equilibrate for five minutes before three consecutive spectra of the samples were collected. Each spectrum is averaged from 8 consecutive scans with a resolution of 16 cm^{-1}. The large resolution can be used because the two asymmetric-stretch features of the nitrate and carbonate ions are able to be resolved with this resolution.

A spectrum of the nitrogen gassed filled long-path cell with the CaF_2 windows was used as the background for the cluster experiments. Three consecutive spectra of the aqueous nitrate cluster samples that were thermally equilibrated to the room temperature (~ 23 ˚C) were collected. Each spectrum is an average of three scans with a resolution of 1 cm^{-1}. To prevent the water clusters from hydrogen bonding the IR windows, an attempt to use Ge windows was made.

2.6 Computational Methods

All calculations were done with the Gaussian 09 electronic structure package[44] on the Western Kentucky University High-Performance Computing Center. Geometry optimization calculations of nitrate and carbonate ions that are hydrated by one (Figure 1.2) and two water molecules (Figure 2.5) were completed with the B3LYP functional,[45] Dunning's correlation-consistent, double- (aug-cc-PVDZ), triple- (aug-cc-PVTZ), and

quadruple-ζ (aug-cc-PVQZ) basis sets.[46] To obtain results that more accurately replicate experimental vibrational frequencies, the Solvation Model based on Density (SMD) was used for calculations in which the nitrate and carbonate ions are hydrated by a single water molecule. B3LYP/aug-cc-PVDZ optimization and vibrational frequency calculations performed by Neumark and coworkers[36] yielded a peak splitting of 50 cm^{-1} in the IR spectrum of nitrate ion, which is observed experimentally. Vibrational frequency analysis of the optimized geometries was completed to determine the difference in the vibrational frequencies of the two asymmetric stretches of the nitrate and carbonate ions. Electronic structure calculations of potential replacements for CCl_4 were performed with B3LYP/aug-cc-PVDZ.

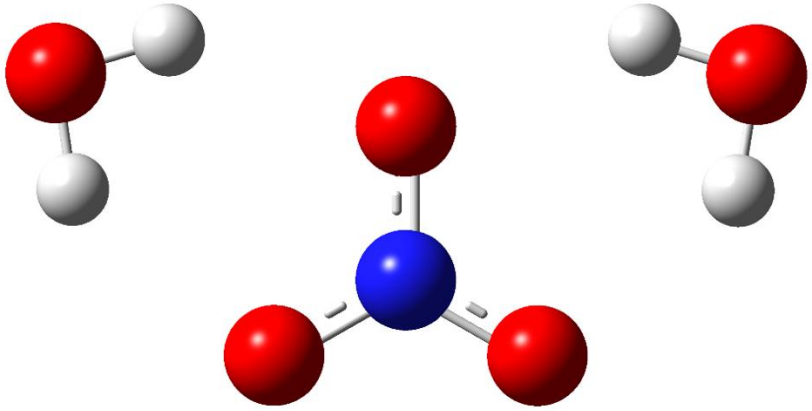

Figure 2.5. Optimized nitrate ion hydrated by two water molecules used for B3LYP/aug-cc-PVDZ vibrational analysis calculations.

3. Bulk Aqueous Nitrate Ion

Recent work conducted by Grassian and coworkers showed that the product ratio from the photolysis of the nitrate ion is dependent on the nitrate concentration in solution.[3] To understand these results on a molecular level, the structure of the nitrate ions needs to be investigated. This may be achieved by identifying the relationship between the ratio of the two nitrate solvation geometries with temperature and ionic concentration of the solution.

3.1 Basic Spectrum and Removal of Water Background

The double peak in the FTIR spectrum of an aqueous 0.1 M KNO_3 solution is presented in Figure 3.1. Both peaks result from the lifted degeneracy of the two asymmetric stretches of the nitrate ion that is induced by the breaking of the D_{3h} symmetry that occurs when the ion is placed in a polar solvent such a water.[36] A collection of raw 0.1 M KNO_3 spectra collected at temperatures between 10 and 50 ˚C are presented in Figure 3.2a. As the temperature of the solution is increased, the absorbance of the low frequency nitrate peak decreases with temperature, which is caused by the tail end of the adjacent temperature-dependent water peak at 1650 cm^{-1}.[47] Because the IR absorbance spectrum of water changes with temperature, a single background cannot be subtracted from each set of nitrate spectra (10 to 50 ˚C). A background that is unique to each sample composition and temperature is required. Temperature-dependent spectra of water between 25 and 50 ˚C in 5˚ C increments, as shown in Figure 3.2b, were collected. In the region of the nitrate asymmetric-stretch peak, the water spectra are approximately linear. Therefore, the absorbance from water can be removed through the subtraction of a linear baseline without actively subtracting the water absorbance at each temperature. The absorbance values of the spectrum at 1200 and 1500 cm^{-1} were used to create a linear baseline that is subtracted

from the KNO_3 spectrum that the two absorbance values were taken. These two positions on the spectrum were chosen because each position lies on one side of the nitrate asymmetric-stretch peak where nitrate does not absorb IR radiation and water does not strongly absorb IR radiation. This process was repeated for each spectrum that was collected at a different temperature to yield a set of spectra, as shown in Figure 3.2c.

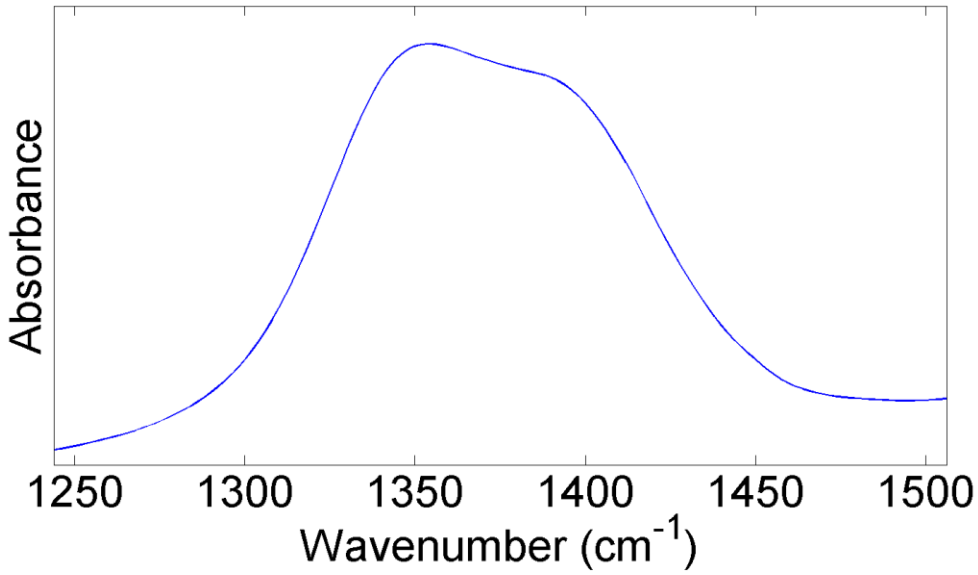

Figure 3.1. Experimental FTIR spectrum of aqueous KNO_3.

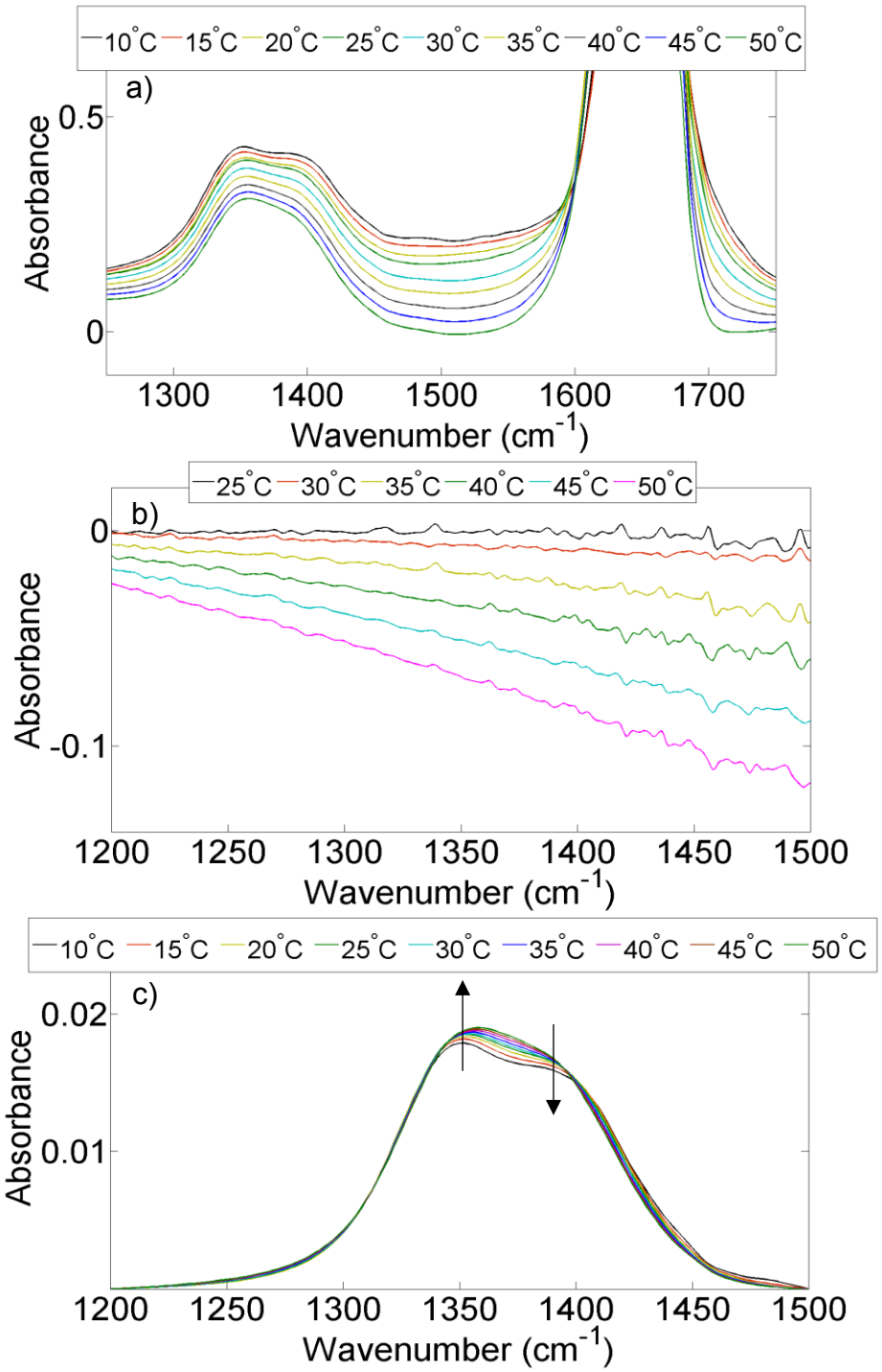

Figure 3.2. Temperature-dependent FTIR spectra of aqueous 0.1 M KNO_3 with the 1650 cm^{-1} water peak (a). Absorbance of IR radiation by water alters the intensity of the nitrate asymmetric-stretch peak. The linear-temperature-dependent FTIR spectra of water in the region of the nitrate asymmetric-stretch peak (b) allows a linear baseline that is specific to each spectrum to be subtracted from the aqueous KNO_3 spectra to produce a set of spectra with the water absorbance removed (c). Black arrows show how the peak intensities change with increasing temperature.

3.2 Temperature Effects

Inspection of the spectra in Figure 3.2c reveals that as the temperature of the solution is increased, the area of the low frequency peak (relative to the area of the high frequency peak) increases as the relative area of the high frequency peak decreases. To interpret this result, B3LYP/aug-cc-PVDZ spectra of the C_s and the C_{2v} nitrate solvation geometries are presented in Figure 3.3. Vibrational frequencies and intensities are convolved with 30 cm^{-1} wide Gaussian peaks. The centers of the two spectra overlap, signifying that the C_s and C_{2v} solvation geometries contribute to each peak in the experimental nitrate IR spectrum in Figure 3.3. In the calculated C_{2v} geometry spectrum, the intensity of the high frequency peak is larger compared to the lower frequency peak. The opposite is true for the calculated C_s geometry spectrum. Changes in the areas of the low and high frequency peaks in the experimental KNO_3 spectra may be interpreted as the conversion of nitrate ions with C_s symmetry to C_{2v} symmetry with increasing temperature, lending to the use of the peaks in the nitrate spectrum as a proxy for the relative amount of each solvation geometry in solution. Contribution of each solvation geometry to each peak in the nitrate IR spectrum prevents the absolute ratio of the two solvation geometries in solution to be determined; only the relative ratio can be determined. Interpretation of the changing peak areas is supported by the presence of two isosbestic points in the UV spectra of aqueous nitrate solutions.[40] The presence of these points are commonly interpreted as the existence of a chemical equilibrium between two species, but they do not unequivocally identify the existence of an equilibrium.[48] Because the structural information of these two species cannot be obtained from the IR or the UV spectra, the C_s and C_{2v} structures may not be an

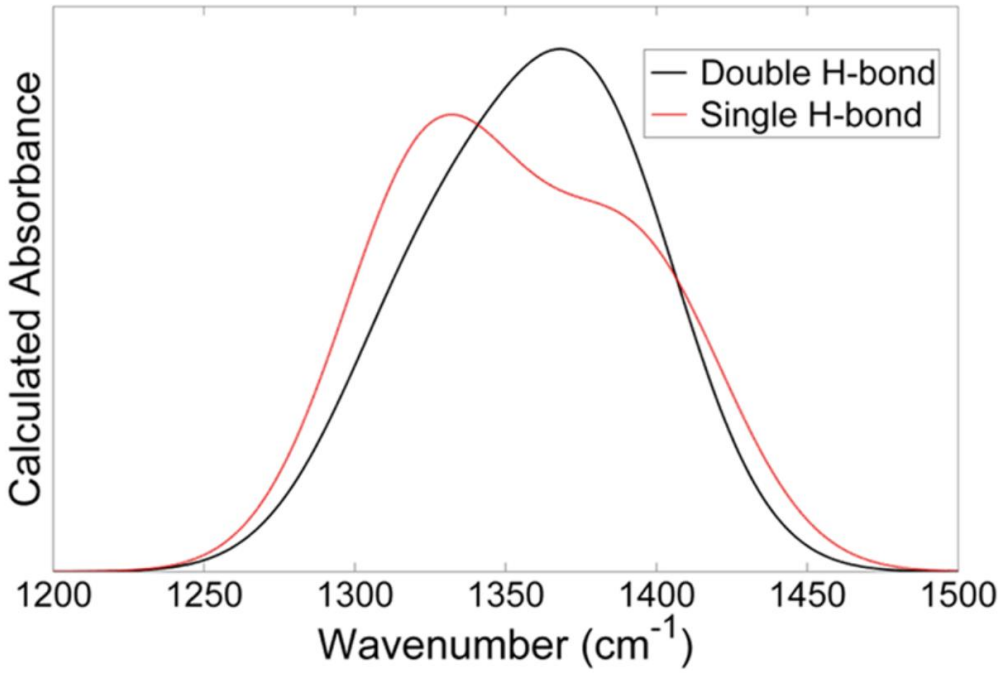

Figure 3.3. B3LYP/aug-cc-PVDZ IR spectra of the singly- (red) and doubly- (black) bound nitrate solvation geometries. Overlap of the spectra show that each solvation geometry contributes to both the low and high frequency peaks in the experimental nitrate spectrum.

accurate representation of the two solvation geometries. Therefore, the two nitrate species are classified as symmetric (C_{2v}) and asymmetric (C_s).

3.3 Analysis of Infrared Nitrate Spectra

To understand on a molecular level why the amount of NO_2^- that is produced from the photolysis of aqueous nitrate solutions increases with the nitrate concentration in solution, the dominant nitrate solvation geometry in solution must be identified. Therefore, the difference in energy between the two nitrate solvation geometries must be determined to identify the energetically favored geometry. A common method that is used to elucidate the difference in energy between two geometries that are in equilibrium is the creation of a van't Hoff plot, which is created by plotting the natural logarithm of the equilibrium constant K_{eq} of the two species (symmetric and asymmetric geometries) that are in chemical

equilibrium as a function of the inverse temperature T of the sample. A least-squares fit of the van't Hoff equation,

$$\ln K_{eq} = -\frac{\Delta_r H^\circ}{RT} + \frac{\Delta_r S^\circ}{R} \quad (1)$$

is fitted to the data points. Here, R is the gas constant, T is the temperature of the solution in Kelvin, $\Delta_r H^\circ$ is the change in enthalpy, and $\Delta_r S^\circ$ is the change in entropy. Error bars for the plots is standard deviation of residuals of the linear fit. Because the areas of the two nitrate peaks are indicative of the relative amount of each solvation geometry in solution, a Gaussian function is fitted to both nitrate asymmetric-stretch features in Figure 3.4 to represent the relative amount of each solvation geometry in solution. The ratio of the integrated areas of these two Gaussian functions is a proxy for the equilibrium constant for the two nitrate geometries while (based on Eq. 1) the slope and the y-intercept of the fit

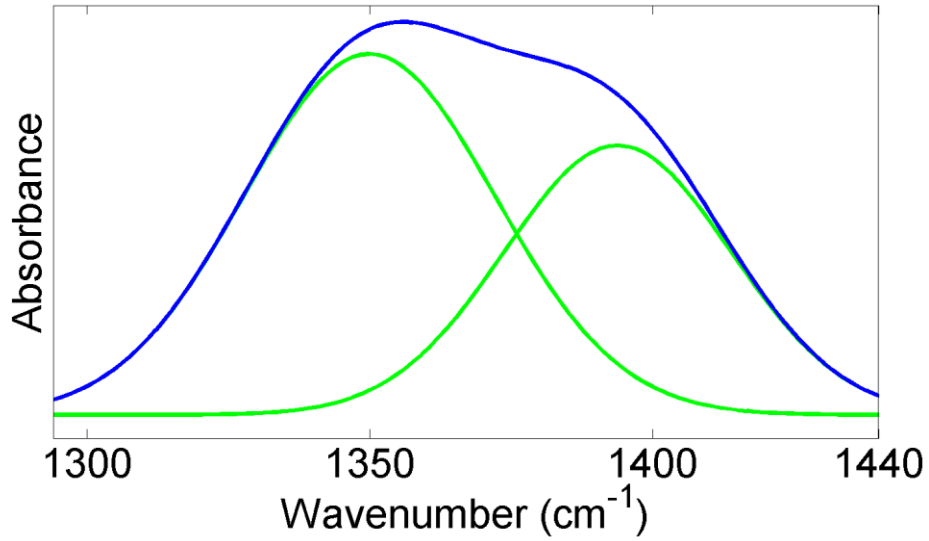

Figure 3.4. A Gaussian function (green line) is fitted to each nitrate asymmetric-stretch peak in the IR nitrate spectrum (blue line). Areas of the two functions are used as a proxy for the relative amount of each solvation geometry in solution. Ratio of the areas of the Gaussian functions are used as the equilibrium constant to create a van't Hoff plot.

line represent $\Delta_r H^\circ/R$ and $\Delta_r S^\circ/R$, respectively. Since this method of analysis is unable to distinguish the extent to which each nitrate solvation geometry contributes to each peak in the experimental nitrate spectrum, the values that are obtained from these plots are relative, but not absolute representations of the two thermodynamic quantities.

To ensure the Gaussian functions are fitted correctly to the asymmetric-stretch nitrate peaks that are present in the IR spectra, the positions and areas of the two peaks were monitored as a function of temperature of the solutions. Conversion from one solvation geometry to the other should manifest as an inversely proportionate relationship between the peak areas of the asymmetric-stretch nitrate peaks (i.e. the increase in the area of one peak should be equivalent to the decrease in the area of the other peak). Shown in Figure 3.5a, as the area of the 1350 cm^{-1} peak (solid blue line) decreases, the area of the 1400 cm^{-1} peak (dashed red line) increases. However, existence of this inverse relationship does not definitively confirm that the Gaussian peaks are correctly fitted to the nitrate asymmetric-stretch peaks. It is possible that this relationship arises because the widths of the Gaussian functions are altered rather than the intensities because the intensities of the peaks change. To ensure the Gaussian functions are accurately fitted to the spectra, it must be confirmed that the peak areas change rather than the peak heights. Furthermore, the peaks widths should approximately be constant because changes in the temperature of the solution do not cause the peaks to broaden. The relationship between the peak areas may arise because the positions of the fitted Gaussian peaks are shifting to yield the lowest fit error. As the temperature of the solutions is changed, the positions of the peaks are expected to red and blue shift, changing the maximum absorbance wavelength, which should be approximately less than 5 cm^{-1}. Shifts in the peak positions that are significantly larger than 5 cm^{-1} are

most likely a result of the shifted Gaussian peaks to produce the lowest fitting error rather than yielding a larger fitting error to correctly fit the two Gaussian functions to the spectra. The relatively stationary positions of the two nitrate asymmetric-stretch peaks with temperature in Figure 3.5b further suggest the analysis of the nitrate spectra is accurate.

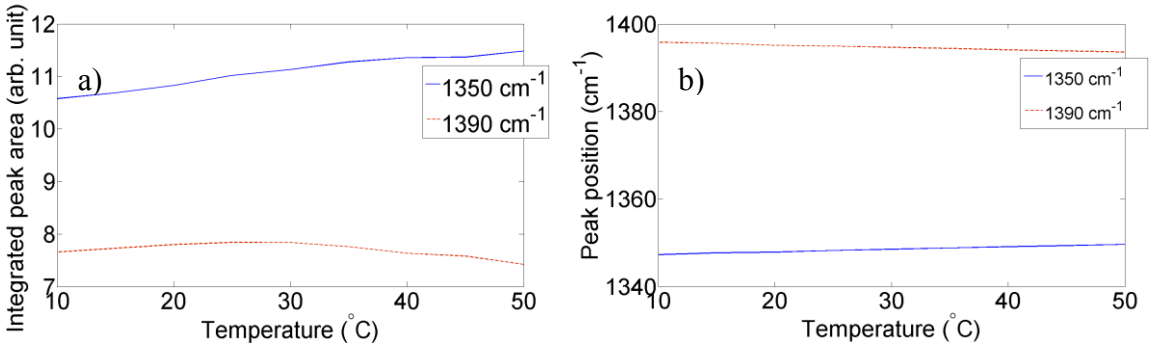

Figure 3.5. Area (a) and position (b) of the high (solid blue line) and low (dashed red line) frequency nitrate peaks in the FTIR spectrum at varying temperatures.

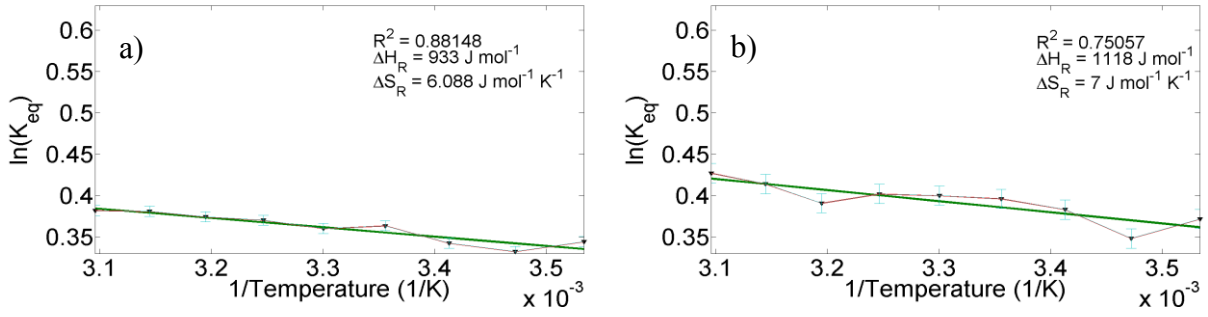

Figure 3.6. Van't Hoff plots for 0.1 M (a) and 0.2 M (b) aqueous KNO_3 solutions. K_{eq} is defined as the ratio of the areas of the two Gaussian functions that are fitted to the infrared spectrum. The slope of the line is representative of $\Delta S^o/R$ and the y-intercept represents $-\Delta H^o/R$. Error bars are the standard deviation of residuals of the linear fit.

3.4 Ionic Strength Effects

Nitrate concentration effects on the relative ratio of the two nitrate solvation geometries is investigated through the comparison of van't Hoff plots in Figure 3.6 for 0.1 M KNO_3 and 0.2 M KNO_3 solutions. Comparison of the plots reveal the 0.2 M KNO_3 solution has a noticeably larger slope compared to the 0.1 M KNO_3 solution, which signifies the difference in energy between the two solvation geometries is larger for the higher nitrate concentration. This increase in energy shows there is a direct relationship between the concentration of nitrate in solution and the difference in energy between the two nitrate ion solvation geometries. The molecular understanding of this relationship cannot solely be determined from these two plots. This change in energy between the nitrate two ion geometries could result from an increase in the ionic concentration in solution or from some competition between the nitrate ions for solvent water molecules. Values of ΔH_R and ΔS_R for aqueous KNO_3 solutions with a total ionic concentration of 0.2 M but different nitrate concentrations are presented in Table 3.1. Each value is averaged from two campaigns (three sets of spectra) that were collected on separate days. Agreement of the values within the uncertainties (the standard deviation of the values from the two campaigns) of the measurements for the two solutions reveals the difference in energy between the two geometries is primarily dependent on the total ionic concentration of the solution. This dependence is believed to arise from the electric fields in solution. As NaCl is added to the solution to increase the ionic concentration of the, the electric fields in solution that are created from water molecules and ions in solution are strengthened. The stronger electric fields may manipulate the geometry of the nitrate ions, by altering the relative stability of the two solvation geometries.

Table 3.1. Values of ΔH_R and ΔS_R for KNO_3 solutions with total ionic concentrations of 0.1 M and 0.2 M.

Sample Composition	ΔH_R (J mol^{-1})	ΔS_R (J mol^{-1} K^{-1})
0.1 M KNO_3	770 ± 91	5.57 ± 0.28
0.2 M KNO_3	893 ± 127	6.20 ± 0.45
0.1 M KNO_3 + 0.1 M NaCl	840 ± 82	6.16 ± 0.27

NaCl was added to the 0.1 M KNO_3 solutions to determine the effects that a wide range of ionic strengths (0.1 to 1.2 M) have on the relative energies of the two solvation geometries. Van't Hoff plots for selected concentrations in Figure 3.7 reveal the y-intercept and the slope of these plots are proportional to the total ionic concentration in solution. The increase in K_{eq} with the total ionic concentration is interpreted as an increase in relative number of nitrate ions with the symmetric geometry compared to the asymmetric geometry in solution. To identify the trend in the relative difference in energy between the two nitrate solvation geometries in solution, the changes in enthalpy and entropy are plotted as a function of the total ionic concentration of the solutions in Figure 3.8. Error bars represent the standard deviation of six measurements collected over two different campaigns. Each campaign was conducted on separate days. Both plots show a linear relationship between the difference in energy of the two solvation geometries and the total ionic concentration of the solution, implying that the electric fields that are in solution are the dominating factors that influence the relative energy of the nitrate solvation geometries in solution over a wide range of ionic concentrations. Moreover, these plots show the symmetric geometry becomes even more favored at higher ionic concentrations compared to the asymmetric geometry. These observations imply the symmetric nitrate ions may be stabilized while the asymmetric nitrate ions may become destabilized with stronger electric fields in solution, which was observed in recent computational work.[49] This may suggest that the symmetric nitrate geometry results in the production of the nitrite ion during photolysis.

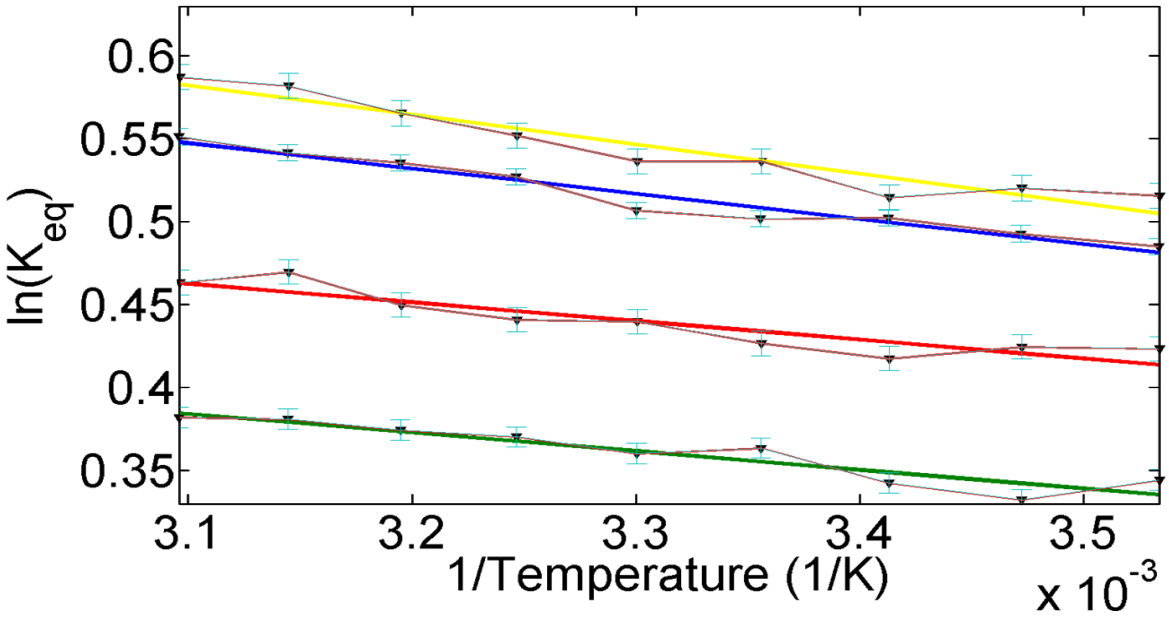

Figure 3.7. Van't Hoff plots of 0.1 M KNO_3 (green), 0.1 M KNO_3/ 0.4 M NaCl (red), 0.1 M KNO_3/ 0.8 M, NaCl (blue), 0.1 M KNO_3/ 1.1 M NaCl (yellow). Error bars are standard deviations of residuals from linear fits.

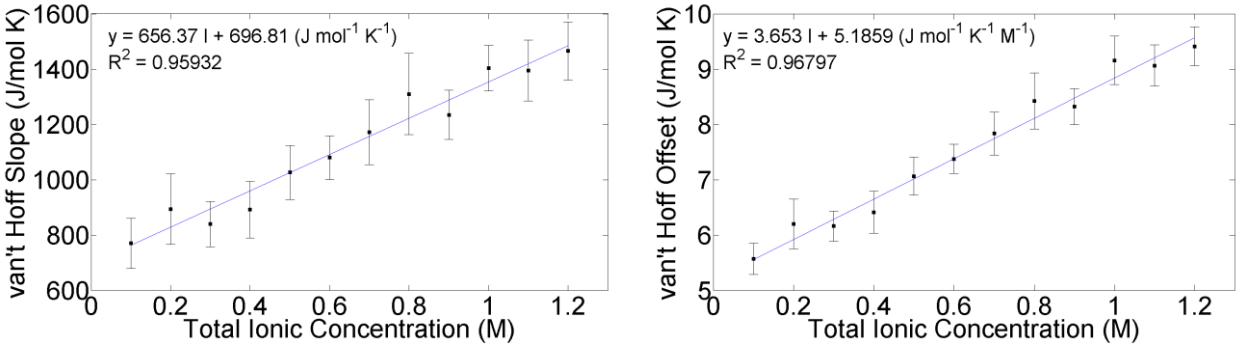

Figure 3.8. Fitted plot of van't Hoff parameters as a function of the total ionic strength of aqueous KNO_3 solutions. Error bars are standard deviations of six independent measurements.

3.5 Conclusions

Evidence shows that the symmetry breaking of the nitrate ion in solution is influenced by the ionic concentration in solution. The data that is presented suggest that the nitrate solvation geometries in solution can be classified as either symmetric or asymmetric. It has been shown that the relative ratio of the two asymmetric stretches of the nitrate ion is dependent on the ionic concentration in solution. More extensive experimental methods (such as multidimensional IR methods) are required to confirm that two nitrate geometries exist in solution.

If the relative ratio of the solvation geometries is dependent on the ionic concentration, the branching ratio during the initial reaction of the photolysis of the nitrate ion may also be dependent on the strength of the electric fields. Therefore, this work may help understand the increased production of NO_2^- from the photolysis of aqueous nitrate with increasing ionic concentration.[3] The effect that more diverse environmental conditions have on the relative ratio of the two nitrate solvation geometries may be determined by investigating the effects that larger ionic concentrations and a wider range of temperatures have on the nitrate geometries. Increased ionic concentrations would be representative of aerosol particles where the limited amount of water causes the ionic concentration to be significantly higher. Expanding the temperature range to 0 to 80 ˚C would also represent more environmental climates that nitrate containing aerosols are found. At extreme temperatures, the relative ratio of the two geometries may experience a plateau effect to which the ratio may remain relatively constant.

4. Bulk Aqueous Carbonate Ion

Dust aerosols are prominent in the atmosphere and influence the climate by contributing to the radiative forcing of the earth[5,50] and altering the lifetime of atmospheric ozone. To determine the magnitude that these particles contribute to radiative forcing effects, which is dependent on the molecules that comprise the particle, compositional changes of these particles with time must be identified. The composition of these particles can change by reacting with molecules (such as ozone) in the atmosphere. Because the reactivity of the particle is partially dictated by the surface composition, the molecules that reside at the surface must be known to predict compositional changes with time. Since the carbonate ion is a primary component of dust aerosols, the location where the carbonate ion resides in the aerosol needs to be known to accurately predict the optical properties of the particle. As for the nitrate ion, the D_{3h} symmetry of the carbonate ion is broken in an aqueous environment, lifting the degeneracy of the two asymmetric stretches of the carbonate ion. Therefore, the carbonate ion is expected to experience the same solvation geometries as the nitrate ion. For reasons that are discussed in Chapter 5, the relative ratio of the solvation geometries may be used to determine the location of the carbonate ions in water clusters, which may help identify where the ion resides in aerosol particles. To elucidate the location of the carbonate ion in the aqueous K_2CO_3 clusters, changes in the relative ratio of the carbonate solvation geometries in the bulk phase with ionic concentration must be first identified.

4.1 Peak Splitting of Asymmetric-Stretch Features

As for the nitrate ion, the D_{3h} symmetry of the isolated carbonate ion causes the two asymmetric stretches of the ion to be degenerate.[51] When carbonate is placed in an aqueous

environment, the symmetry of the carbonate ion is broken, causing the degeneracy of the two asymmetric stretches to be lifted, which manifests as a separation of the two asymmetric-stretch peaks in the IR spectrum. Compared to the nitrate ion spectrum, the magnitude of the peak splitting in the raw 0.1 M K_2CO_3 spectrum of Figure 4.1 is reduced, causing the two asymmetric-stretching features in the carbonate spectrum to appear as a single peak. One-dimensional IR spectra of sodium nitrate, sodium carbonate, and water that were collected by Tokmakoff and coworkers[52] report the difference in the magnitude of the peak splitting for nitrate results from stronger hydrogen bonds (H-bonds) between the solvating water molecules and the carbonate ion, which is also supported by two dimensional (2D) IR spectra of sodium carbonate. Compared to the carbonate ion and water molecules, the weaker interactions between the nitrate ion and water molecules allows the H-bonds between the nitrate ion and the water molecules to be more easily broken, resulting in a highly fluctuating solvation shell around the ion. This continually changing solvation shell induces a large distribution of NO stretches that manifest as a large peak split in the IR spectrum. Contrarily, the stronger H-bonds between the carbonate ion and the water molecules prevents rapid changes to the solvation shell. Consequently, there is a smaller distribution of CO vibrational frequencies that manifests as a smaller peak splitting in the IR spectrum. The reduced splitting makes fitting a Gaussian function to the two asymmetric-stretch features difficult because two Gaussian functions may be fitted to the IR spectrum in multiple ways that yield low fit errors. However, neither the positions nor the areas of the Gaussian functions may accurately represent the two asymmetric stretching features in the spectrum even if the fit results in a low error.

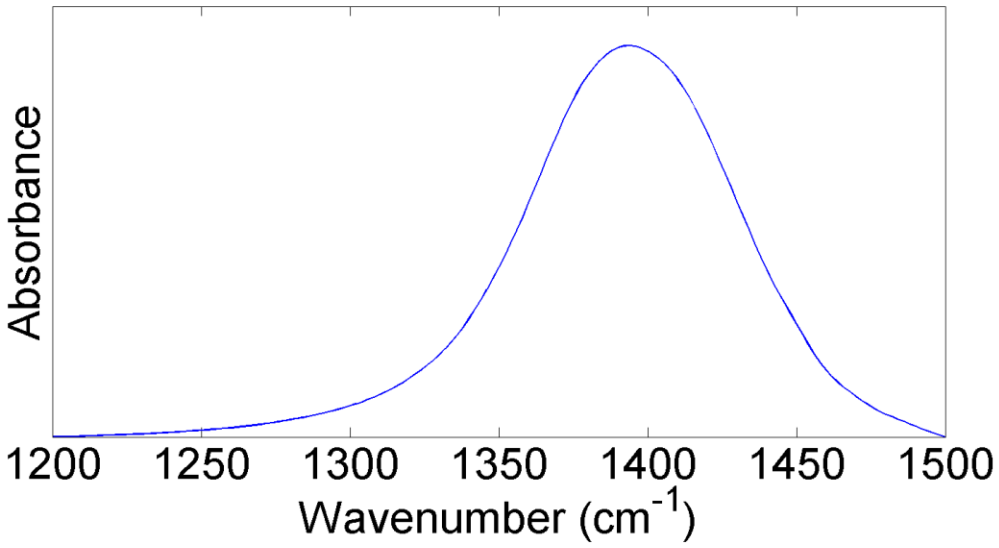

Figure 4.1. FTIR spectrum of aqueous K_2CO_3 in the asymmetric-stretching region.

To alleviate the difficulty of correctly fitting two Gaussian functions to the carbonate asymmetric-stretch peak, the vibrational frequencies of the nitrate and carbonate ions solvated by two water molecules were calculated with the B3LYP functional[45] using the aug-cc-PVDZ, aug-cc-PVTZ, and aug-cc-PVQZ basis sets.[46] Scaled peak splitting values and scaling factors[53] are presented in Table 4.1. Calculations of the doubly-hydrated nitrate ion serves as a standard because the experimental peak splitting for the nitrate ion is known and the calculated peak splitting that is reported for this structure agrees with the experimental value.[36] Since the nitrate and carbonate ions are isoelectronic and have a D_{3h} symmetry in the gas phase, it reasonable to expect that the calculated peak splitting for the carbonate ion that is hydrated by two water molecules should be representative of the experimental peak splitting of the carbonate ion. Using the aug-cc-PVDZ geometry

optimized nitrate ion that is hydrated by two water molecules as a starting geometry for the carbonate ion hydrated by two water molecules, the calculated peak splitting for the carbonate ion is 45.82 cm^{-1}.

Table 4.1. Scaled peak splitting values for B3LYP carbonate ions solvated by two water molecules obtained with different basis sets.

Level of Theory	Scaling Factor	Nitrate (cm^{-1})	Carbonate (cm^{-1})
Experimental		50	32
aug-cc-PVDZ	0.9713	49.34	45.82
aug-cc-PVTZ	0.9687	50.90	33.22
aug-cc-PVQZ	0.9685	51.39	39.70

The small difference between the calculated peak splitting for the carbonate ion and the experimental splitting for the nitrate ion suggest that the calculated splitting for the carbonate ion is not physically reasonable. If the splitting of the two carbonate asymmetric-stretch features is 45.82 cm^{-1}, the two features would be distinguishable, as they are in the nitrate spectrum. Therefore, a larger basis set is needed for the carbonate ion calculation. The aug-cc-PVDZ and aug-cc-PVTZ basis sets were used to perform the same calculation for the doubly-hydrated nitrate ion structure to ensure a peak splitting that is physically reasonable is obtained. For both basis sets, the nitrate peak splitting is approximately 50 cm^{-1}, suggesting that these basis sets are large enough perform the calculation for the carbonate ion. Peak splitting values for the doubly-hydrated carbonate ion that are obtained from the aug-cc-PVTZ and aug-cc-PVQZ basis set calculations lie between 33 and 40 cm^{-1}, which are physically reasonable because the two asymmetric-stretch features that have a splitting that is less than 40 cm^{-1} should not be visually distinguishable in the IR spectrum. Because it is not possible to visually determine if the magnitude of the splitting of the carbonate asymmetric-stretching features is 33.16 or 39.22 cm^{-1}, further analysis of the K_2CO_3 spectra is required. It is important to note that the nitrate ion that is hydrated by two

water molecules is a transition state[36] while the equivalent structure for the carbonate ion is a minimum energy structure. The effect that this difference in the energy structures has on the magnitude of the peak splitting is not known and could mean that the peak splitting for the carbonate ion that is hydrated by two water molecules is not representative of the experimental peak splitting.

4.2 Analysis of K_2CO_3 Spectra

As for the raw aqueous KNO_3 spectra, the water peak at 1650 cm^{-1} alters the line shape of the carbonate ion peak in Figure 4.2a. To monitor the changes in the relative ratio areas of the two carbonate asymmetric-stretching features without the influence of the water spectra, the contribution from water needs to be removed from the K_2CO_3 spectra using the same procedures that were used for the analysis of the KNO_3 spectra. Aqueous K_2CO_3 IR spectra, with the water absorbance removed, is shown in Figure 4.2b. For the Gaussian functions that are fitted to the carbonate spectra to accurately represent the positions of the two asymmetric-stretch peaks of the carbonate ion, the fitting parameters (the initial guess of the locations where the two Gaussian functions should be located (Start Guess) and the distance from the initial guesses that the functions can be fitted (Window)) in the custom-built Matlab[54] peak fitting program need to be optimized for the aqueous K_2CO_3 spectra.

Because the carbonate and nitrate ions are isoelectronic and have a D_{3h} symmetry in the gas phase, the two carbonate solvation geometries are expected to follow the same in Table 4.2 are expected to be similar. Combinations of parameters that produce peak position, area, and/or height ratios for the carbonate ion that deviate from the equivalent nitrate ion ratio by 15% or more are deemed to be excessively small or large compared with the true value, signifying that the combination of parameters is not appropriate to

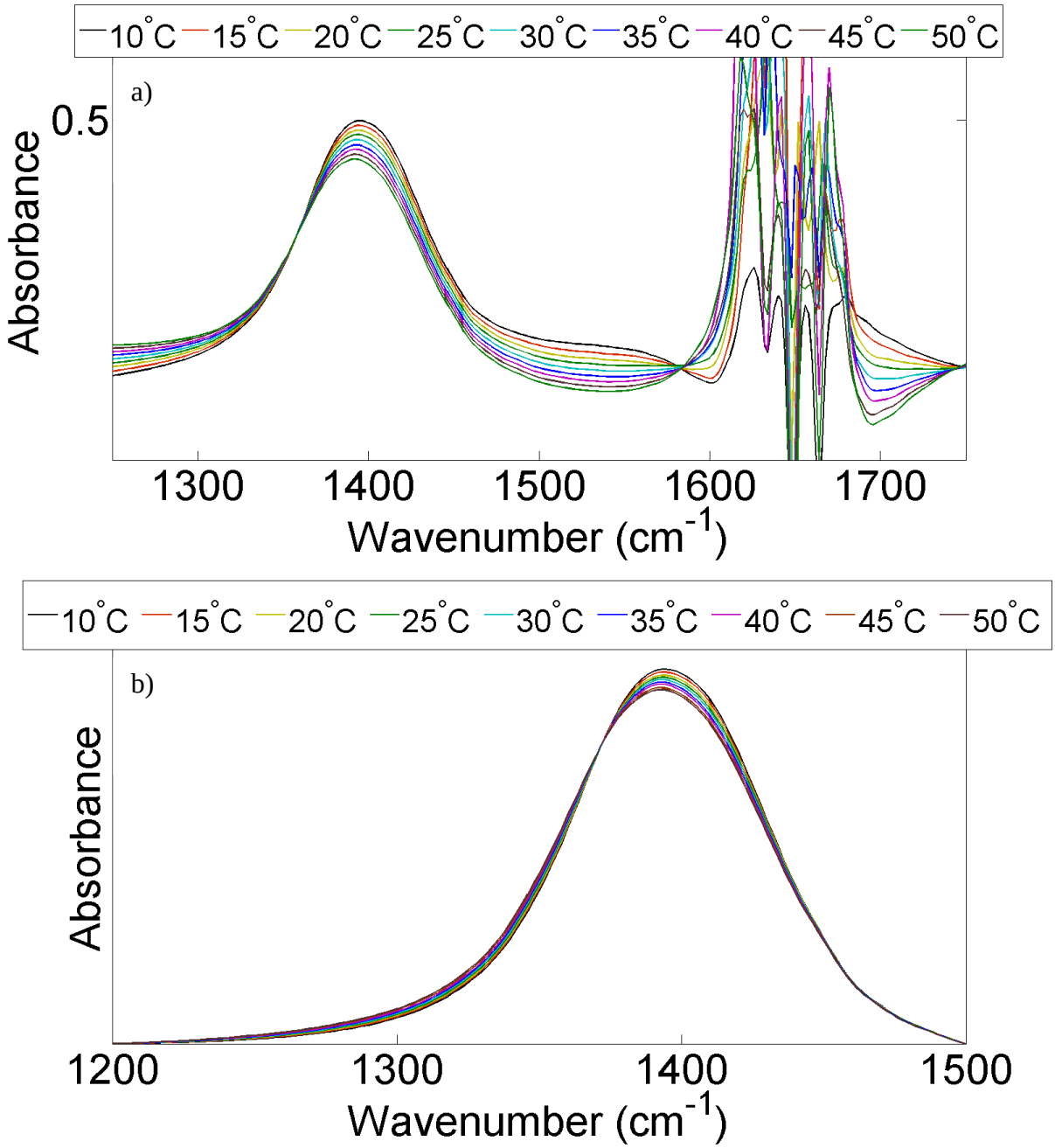

Figure 4.2. Temperature-dependent FTIR spectra of the 0.1 M K_2CO_3 asymmetric-stretch peak the adjacent water peak (a) and the water absorbance removed (b).

correctly with the true value, signifying that the combination of parameters is not appropriate to correctly fit two Gaussian functions to the carbonate peak. Combinations of parameters are further rejected by eliminating sets that produced a van't Hoff plot with a low R^2 value (below 0.9); low R^2 values indicate that the combination of parameters is not correct for the analysis of the spectra. This leaves sets 1 and 5 as the only ones that have not been eliminated. Comparison of the peak splitting values that were obtained from sets 1 and 5 to the aug-cc-PVTZ calculated splitting reveals a good agreement between the calculated splitting and the splitting that was obtained from set 5, suggesting that this set is correct. Because the calculated peak splitting values for the carbonate ion that are presented in Table 4.1 do not coincide with one another, the close agreement between the values that was obtained from the B3LYP/aug-cc-PVTZ calculation and the peak fitting program may be coincidental. Therefore, the two combinations of parameters in sets 1 and 5 were used to analyze each set of temperature-dependent K_2CO_3 spectra. The slopes and offsets of the van't Hoff plots that were created with the parameters in sets 1 and 5 are plotted as a function of the total ionic concentration of the solution in section 4.4. The presence of a strong linear trend in the plots that are created with the parameters in set 5 and the absence thereof in the plots created with the parameters in set 1 supports the conclusion that a window of 120 is correct to fit two Gaussian functions to the carbonate peak.

4.3. Temperature Effect

Interrogation of the aqueous temperature-dependent K_2CO_3 spectra with the water absorbance removed in Figure 4.3 reveals that the two unresolved asymmetric-stretch peaks hinder the temperature effects on the relative ratio of the two carbonate solvation

geometries being visually identified in the spectra. The integrated peak areas of the fitted Gaussian functions with temperature need to be plotted, as in Figure 4.3, to identify the temperature effects. As for the KNO_3 solutions, the integrated areas of the fitted Gaussian peaks are inversely proportional, suggesting that one carbonate solvation geometry is being converted to the other as the temperature of the solution changes. Interestingly, as the temperature of the K_2CO_3 solution increases, the area of the low frequency peak (relative to the area of the high frequency peak) decreases as the area of the high frequency peak increases. The calculated IR spectra of the nitrate ion singly- and doubly-bound to a water molecule in section 3.2 shows that the singly-bound nitrate geometry contributes more to the low frequency peak and the doubly-bound nitrate geometry contributes more to the high frequency peak. Because nitrate and carbonate are isoelectronic and have a D_{3h} symmetry in the gas phase, it is reasonable to expect that the same carbonate solvation geometries contribute to the same frequency peaks. Therefore, the change in the carbonate peak areas may be interpreted as the relative amount of carbonate ions with the asymmetric geometry decreases while the relative amount of carbonate ions with the symmetric solvation geometry increases. This result is unexpected because the symmetric nitrate geometry has been shown to be lower in energy than the asymmetric nitrate geometry. It is reasonable to expect that the symmetric carbonate geometry is lower in energy than the asymmetric carbonate structure, implying that the relative amount of carbonate ions with the asymmetric geometry should increase with temperature. To investigate this occurrence, electronic structure calculations of the carbonate ion that is hydrated by a single water molecule were completed. Minimum energy structures calculations for the carbonate ion doubly- (symmetric) and singly-bound (asymmetric) to a water molecule were performed

Table 4.2. Values of the Gaussian functions that are fitted to the K_2CO_3 spectra for the fitting parameters set to different values. The different combinations of values are categorized into sets. The combinations of parameters that may be correct for the analysis of the K_2CO_3 FTIR spectra are indicated by *.

Compound	Set	Window	Start Guess (cm^{-1})	Peak Height Ratio	Peak Area Ratio	Peak Splitting (cm^{-1})	R^2
KNO_3		150	1380, 1410	1.339	1.483	50	
K_2CO_3	1*	80	1380, 1410	1.249	1.420	25	0.84098
K_2CO_3	2	90	1380, 1410	1.179	1.272	27	0.93863
K_2CO_3	3	100	1380, 1410	1.595	2.100	29	0.97816
K_2CO_3	4	110	1380, 1410	1.536	1.923	31	0.98453
K_2CO_3	5*	120	1380, 1410	1.384	1.608	33	0.98620
K_2CO_3	6	130	1380, 1410	1.200	1.268	34	0.9850
K_2CO_3	7	140	1380, 1410	1.714	2.111	35	0.96977
K_2CO_3	8	150	1380, 1410	1.691	2.005	36	0.96848

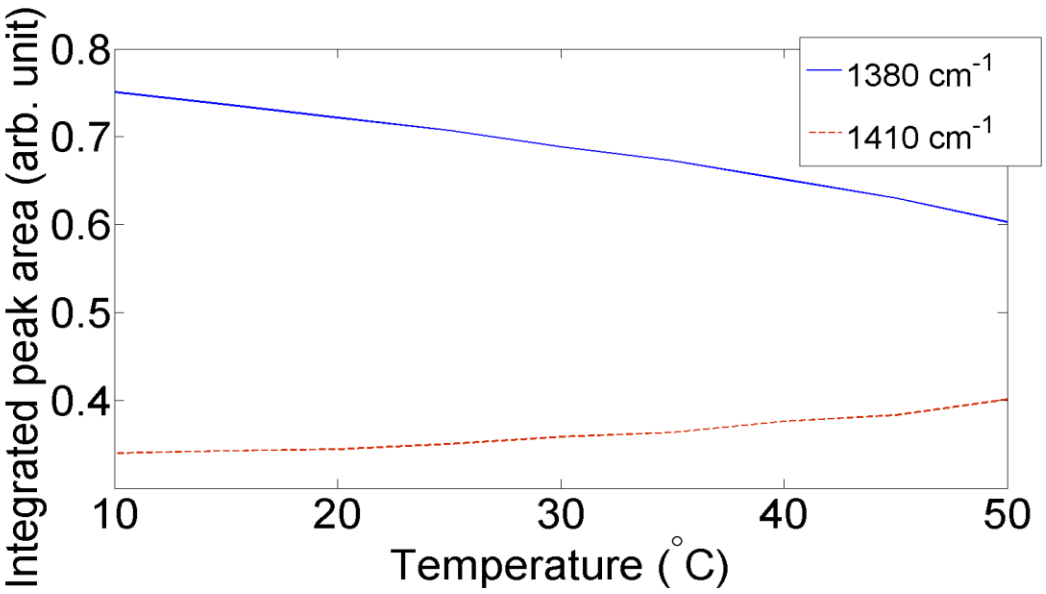

Figure 4.3. Integrated peak areas of the high frequency (solid blue line) and low frequency (dashed red line) features of the K_2CO_3 spectra as a function of temperature.

with B3LYP/aug-cc-PVDZ. In agreement with structures that are reported in the literature, a minimum energy structure for the symmetric geometry was found, but not for the asymmetric carbonate geometry.[55,56] All attempts to find a minimum energy structure for the singly-bound geometry resulted in the formation of a bicarbonate ion and the hydroxyl radical. When the SMD[57] is applied to the singly-bound carbonate ion, a first-order transition state is found. These results suggest that the singly-bound carbonate structure may not be an accurate representation of the carbonate solvation geometry that is present in solution. The issue may be that the calculations have been performed for a planar carbonate ion. Electronic structure calculations of the carbonate ion in water suggest that the planarity of the ion is broken in solution.[2] Therefore, the next step is to search for minimum energy structures for a nonplanar carbonate solvation structure that is hydrated

by a single water molecule and determine the relative energy of the global minimum structures.

4.4 Ionic Concentration Effects

Van't Hoff plots for aqueous 0.1 M K_2CO_3 solutions with varying total ionic concentrations are presented in Figure 4.4. Plots that were created with a Window of 120 are only shown because it is believed to be the correct value for the analysis of the K_2CO_3 spectra. Error bars are the standard deviations of the residuals of the linear fit. Sodium chloride was added to the solutions to increase the total ionic concentration. Interestingly, the slope of the plots is positive, meaning the relative amount of carbonate ions with the symmetric geometry increases with temperature. Further inspection of the plots reveals that

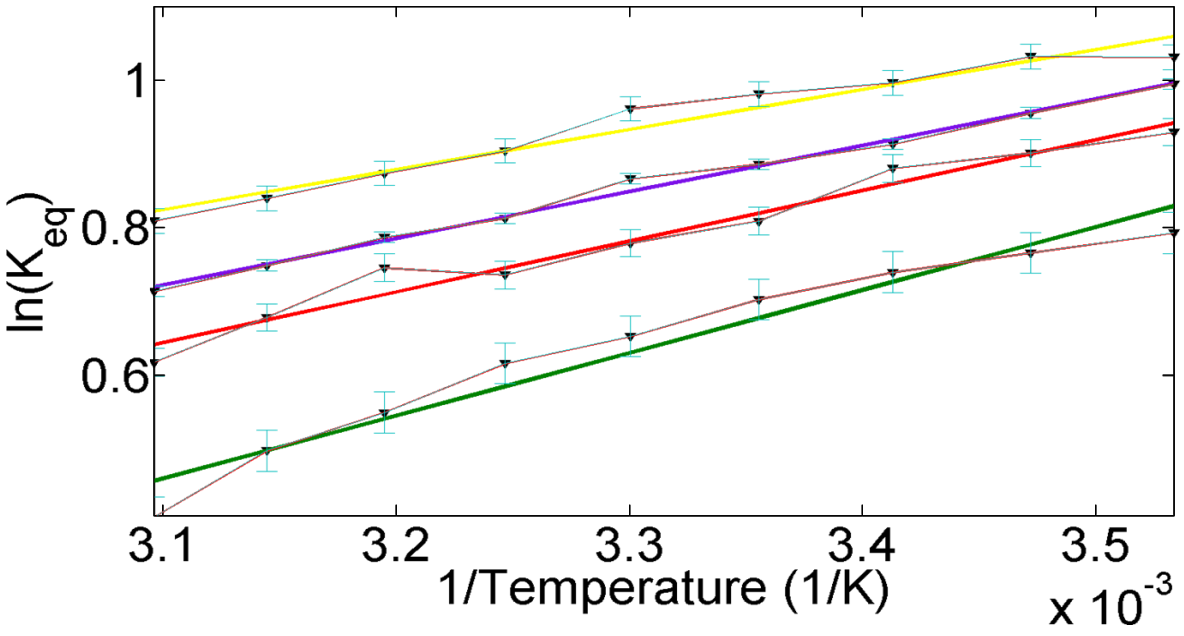

Figure 4.4. Van't Hoff plots of 0.1 M K_2CO_3 (green), 0.1 M K_2CO_3/ 0.4 M NaCl (red), 0.1 M K_2CO_3/ 0.8 M, NaCl (blue), and 0.1 M K_2CO_3/ 1.1 M NaCl (yellow). Error bars are the standard deviations of residuals from linear fits.

the slopes are significantly larger compared to the plots for KNO_3, indicating more energy is required to convert between the two carbonate solvation geometries. This increase in energy may be explained by the relative strength of the hydrogen bonds. One- and two-dimensional IR spectra of aqueous $NaNO_3$ and Na_2CO_3 that were collected by Shen, et al. suggest that the H-bonds between the carbonate ion and water molecules are stronger than the H-bonds between the nitrate ion and water molecules.[52] As the asymmetric carbonate structure converts to the symmetric carbonate geometry, more energy is released compared to the nitrate ion because of the stronger H-bonds.

To identify the effects that the ionic strength has on the relative ratio of the two solvation geometries in solution, the slopes and offsets of the van't Hoff plots are plotted as a function of the total ionic concentration. Because the same plots for the KNO_3 samples display a strong linear relationship, which indicates that the difference in energy between the two solvation geometries is primarily dependent on the total ionic concentration, it is reasonable to expect that the difference in energy between the two carbonate solvation geometries is primarily dependent on the ionic concentration. This dependence should manifest a strong linear relationship in the plots of the slope and offset of the van't Hoff that are plotted as a function of the total ionic concentration. The presence or absence of a strong linear trend in these plots for the aqueous K_2CO_3 solution should also help identify which combination of fitting parameters that were isolated in section 4.2 are correct for the analysis of the aqueous K_2CO_3 spectra. As shown, the plots that are created with the fitting parameters in set 1 show a weaker linear relationship than the plots that were created with fitting parameters in set 5. The stronger linear relationship that is present in Figures 4.5a and b suggest that the combination of fitting parameters in set 5 are most correct to fit a

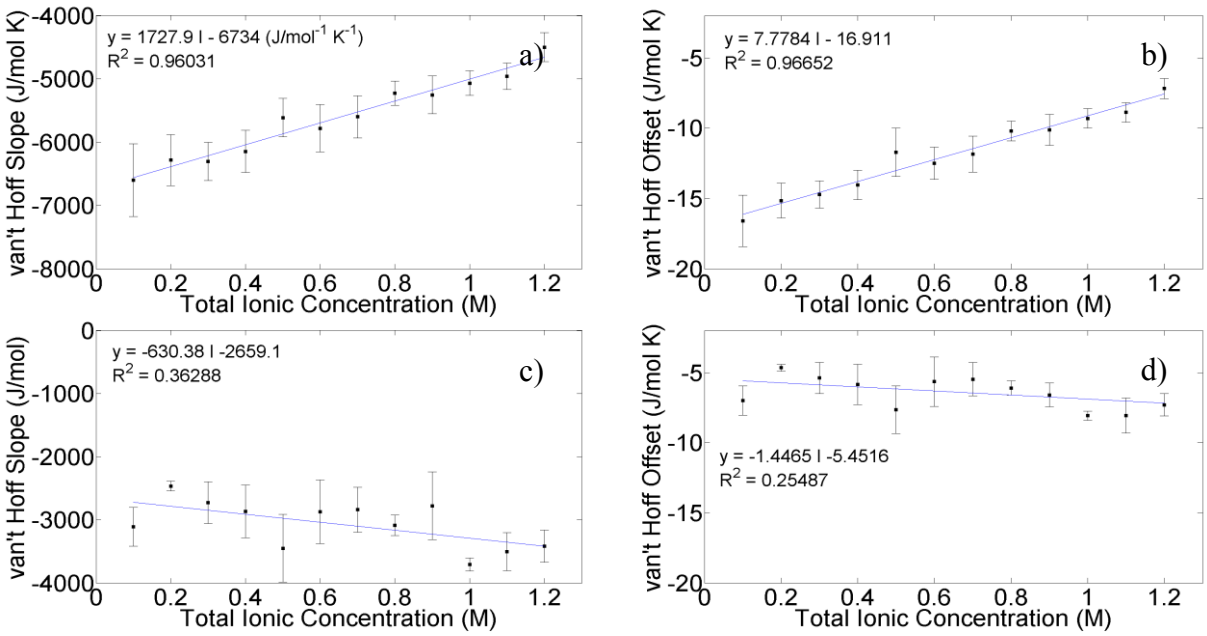

Figure 4.5. Plots of ΔH and ΔS as a function of the total ionic strength of aqueous K_2CO_3 solutions obtained for fitting parameters 5 (a and b) and 1 (c and d) of Table 4.2. Error bars are the standard deviations of six independent measurements.

Gaussian function to the two asymmetric-stretch features in the aqueous K_2CO_3 FTIR spectra.

The linear trend also implies the lower energy structure (asymmetric geometry) is destabilized by strong electric fields. This could mean the asymmetric carbonate geometry may be favored in the high ionic concentration environments of aerosol particles. Because the aerosol-air interface is an asymmetric solvation environment, it is reasonable to expect the asymmetric carbonate solvation geometry is favored at the aerosol surface. The asymmetric carbonate geometry that is stabilized by the high ionic concentrations in the aerosols may be drawn to the asymmetric solvation environment at the aerosol surface. Investigation into the location of carbonate ions in aerosol particles may be done by probing aqueous carbonate clusters.

4.5 Conclusions

Evidence shows that the symmetry breaking of the carbonate ion in solution is influenced by the ionic concentration in solution. If two solvation geometries or two classes of geometries are present in solution, the electronic structure calculations for the carbonate ion that is hydrated by a single water molecule questions the accuracy of the two proposed solvation geometries for the carbonate ion. A more thorough search for minimum energy structures for the carbonate ion hydrated by a single water molecule is required to ensure no minimum energy structures for an asymmetric carbonate solvation geometry exist. The work that is presented may help elucidate the surface composition of dust particles. Once it is known how the ionic strength in solution affects the stability of the carbonate solvation geometries in the bulk phase, the stability of the solvation geometries in room temperature water clusters can be investigated. Results from these experiments will help reveal the preferred location of the carbonate ions in aerosols.

Because the analysis of the aqueous K_2CO_3 FTIR spectra is influenced by the analysis of the aqueous KNO_3 FTIR spectra (the analysis of the K_2CO_3 spectra is tailored so that similar trends are observed between K_2CO_3 and KNO_3 spectra), more work is required to confirm the positions of the two carbonate asymmetric-stretch features to ensure that the analysis of the K_2CO_3 spectra is correct. This may be achieved by collecting IR spectra of high ionic strength carbonate solutions. The magnitude of the peak splitting of the two nitrate asymmetric-stretch features in aqueous $Ca(NO_3)_2$ has been shown to be proportional to the ionic concentration of the solution.[6] At high ionic concentrations, the two carbonate asymmetric-stretch features are expected to become resolved. Incrementally increasing the ionic concentration would allow the trend between the ionic concentration and the

magnitude of the peak splitting to be identified, potentially allowing the peak splitting for ionic concentrations that are below 1 M to be predicted. Identification of the peak splitting for low ionic concentration carbonate solutions would allow the analysis of the K_2CO_3 spectra to be confirmed. The relative stability of the two carbonate solvation geometries may be investigated through the collection of IR spectra of aqueous K_2CO_3 clusters. As it is discussed in Chapter 5, the two nitrate asymmetric-stretch features for the aqueous KNO_3 clusters are significantly narrower compared to the bulk aqueous KNO_3 samples. If the same effect is observed for the aqueous K_2CO_3 solution, the changes to each asymmetric-stretch feature will be more easily identified compared to the bulk phase.

5. Aqueous Nitrate Ion Clusters

Water is the most prevalent solvent on earth. It has applications in multiple disciplines such as chemistry, biology, cooking, and many other fields. Despite its ubiquity, the interactions between water molecules and solvated compounds are not well characterized. When a molecule is placed in a solvent, the compound becomes surrounded by multiple solvent molecules to create a solvation shell, which influences the solvated molecule. The effect that this shell has on the solute species is dependent on the identity of the solute and solvent molecules. This encapsulation of the solvated compound is important to understand because it influences the chemical processes that the compound undergoes.[58] In bulk-liquid solutions, multiple solutes of varying identities are present, making it difficult to solely interrogate the effects that the solvent molecules have on a single type of solute molecule. Investigation into the pure solute-solvent interactions has been made possible through the ability to create and probe clusters of atoms and molecules. Control over the composition of the clusters allows the pure solute-solvent interactions to be probed.

5.1 Preliminary Results in Carbon Tetrachloride

5.1.1 Magnitude of peak splitting

FTIR spectra of CCl_4 (blue), bulk aqueous KNO_3 (yellow) and aqueous KNO_3 clusters immediately (red) and three weeks (black) after the aqueous KNO_3 cluster sample was prepared are presented in Figure 5.1. Black arrows indicate the positions of the nitrate asymmetric-stretch peaks in the aqueous KNO_3 cluster spectra. Because each spectrum is vertically displaced to easily compare the relative peak height ratios between spectra, comparison of the intensities of the peaks between the spectra is not meaningful. Interestingly, the ~12 cm^{-1} splitting of the two nitrate asymmetric-stretch peaks for the

aqueous cluster sample is significantly reduced compared to the 50 cm^{-1} peak splitting that is observed in the bulk phase. The decreased peak splitting is believed to result from the reduced number of water molecules (compared to the bulk phase) that surround each nitrate ion, which is supported by the decreased full width at half maximum (FWHM) of the nitrate asymmetric-stretch peaks, or the decreased ionic concentration in the sample. In the bulk phase spectra, the two asymmetric-stretch features are largely broadened (large FWHM) because of the large distribution of nitrate ions that experience slightly different solvation environments that shifts the vibrational frequencies of the two asymmetric stretches of the nitrate ion. Reducing the number of water molecules that surrounds the nitrate ions, as in the aqueous KNO_3 clusters, limits the number of configurations around the nitrate ion that the water molecules can be arranged. This limits the number of solvation environments that the nitrate ions experience, which induces a smaller distribution of vibrational frequencies.

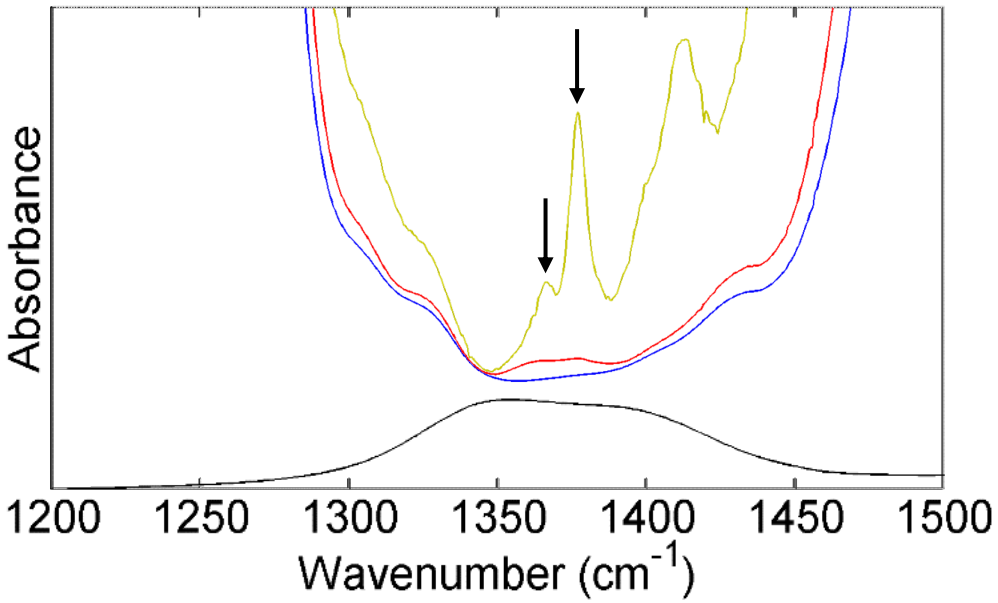

Figure 5.1. FTIR spectra of CCl_4 (blue), bulk aqueous KNO_3 (brown) and aqueous KNO_3 clusters immediately after (red) and three weeks after (yellow) the sample was prepared. The black arrows indicate the positions of the nitrate asymmetric-stretch features.

frequencies of the nitrate ion, manifesting as a reduction in the FWHM of the asymmetric-stretch peaks.

Experimental work performed by Neumark and coworkers also supports the argument that the decreased peak splitting results from the reduced number of water molecules in the sample.[36] To investigate the impact that individual water molecules have on the magnitude of peak splitting of the nitrate ion in the IR spectrum, IRMPD spectroscopy was used in the study to probe mass selected nitrate ions that were hydrated by one to six water molecules. The peak splitting of the two nitrate asymmetric-stretch nitrate peaks in the IRMPD spectra were monitored for each cluster size. Nitrate ions hydrated by four water molecules exhibit a peak splitting of 12 cm^{-1}, which is consistent with the peak splitting in the FTIR spectra of the aqueous KNO_3 clusters. This agreement in the splitting between the IRMPD spectrum and the FTIR spectra of aqueous KNO_3 clusters suggest that the nitrate ions in the aqueous clusters presented here may be hydrated by four water molecules. Alternatively, the reduced peak splitting could result from the decreased ionic concentration in the sample. Grassian and coworkers have shown that the magnitude of the peak splitting of the nitrate asymmetric-stretch features is dependent on the nitrate concentration of the solution.[6] In Chapter 3, it was shown that this effect is primarily dependent on the ionic concentration in the solution. In the aqueous KNO_3 cluster samples, the ionic concentration in the solution is significantly reduced compared to the bulk phase because fewer ions are present in the sample. To determine the impact that low ionic concentrations has on the magnitude of the peak splitting of the nitrate asymmetric-stretch features, the bulk phase experiments that are presented in Chapters 3 and 4 needs to be repeated for nitrate concentrations that are experienced in the cluster samples. Results from

this experiment will allow the primary cause (reduced number of solvating water molecules or reduced ionic concentration) for the reduction of the peak splitting in the nitrate IR spectrum to be identified.

5.1.2 Relative Ratio of the Nitrate Solvation Geometries

Comparison of the relative heights of the absorbance peaks in Figure 5.1 reveals that the area of the low frequency peak in the bulk phase spectrum is larger than the high frequency peak and the opposite is true for the aqueous KNO_3 cluster spectra. Based on the results that are described in Chapter 3, the difference in the peak areas indicate that more nitrate ions experience a symmetric solvation geometry in the bulk phase while more nitrate ions experience an asymmetric solvation geometry in the aqueous clusters. The difference in the peak height ratios may result from different arrangements of the water molecules around the nitrate ion. To interpret the IRMPD spectra of microhydrated nitrate ions on a molecular level, Neumark and coworkers also performed electronic structure calculations for the nitrate ion hydrated by one to six water molecules.[36] For each cluster size, geometry optimization calculations followed by vibrational frequency calculations were performed to find minimum energy isomers. Inspection of the IRMPD spectrum of the nitrate ion that is hydrated by four water molecules reveals two maxima at 1345 and 1357 cm^{-1}, as in the FTIR spectra of KNO_3, with a peak splitting of 12 cm^{-1} and a shoulder located around 1395 cm^{-1}. The intensity of the shoulder is half of the two maxima peaks. The 12 cm^{-1} peak splitting was not able to be reproduced by the electronic structure calculations, suggesting that an unidentified isomer exist; however, the position of one of the nitrate asymmetric-stretch peaks (1388 cm^{-1}) for one of the calculated isomers agrees well with the position of the shoulder that is present in the IRMPD spectrum. This agreement was interpreted as the

isomer that resulted in the two maximum peaks is doubly abundant compared to the isomer that causes the shoulder at 1395 cm^{-1}. Because the calculations done by Neumark and coworkers suggest that multiple isomers exist in the gas phase, it is reasonable to expect that multiple isomers also exist in the aqueous KNO_3 clusters in unequal proportions, meaning that one isomer is more abundant in the sample. Because of the different arrangements of water molecules around the nitrate ion, it is reasonable to expect that each isomer favors either the symmetric or asymmetric solvation geometry, causing one of the nitrate solvation geometries to be more abundant in the sample. Consequently, the peak area that results from the most prominent nitrate solvation geometry in the FTIR spectrum will be a larger relative to the other nitrate asymmetric-stretch peak.

If the interpretation that the nitrate ions are surrounded by four water molecules is incorrect, but the ions are hydrated by a larger number of water molecules, the difference in the peak height ratios may be a result of the size of the aqueous KNO_3 clusters that are dispersed in the CCl_4. Gerber and coworkers performed molecular dynamic (MD) simulations to investigate the location of a nitrate ion in water clusters that range from 15 to 500 water molecules.[59] For clusters composed of 15 to 300 water molecules, the nitrate ion showed a propensity to reside at the exterior of the cluster while the ion became solvated in the interior of the cluster that are composed of more than 300 water molecules. Inherently, the solvation environments at each location in the cluster are different. At the exterior of the cluster, the ion is located at the interface of two phases (the water cluster and the surrounding medium), creating an asymmetric solvation environment. In the interior of the cluster, the ion is surrounded by only water molecules, creating a more symmetric solvation environment. Because of the difference in the two locations, it is

reasonable to expect that the symmetric solvation geometry is favored at the interior while the asymmetric geometry is favored at the exterior. Because the sizes of the clusters that are dispersed in the CCl_4 are not known, the location of the nitrate ions in the clusters is also unknown. Despite the primary location of the nitrate ions in the clusters, the more abundant solvation geometry results in a larger area of the corresponding asymmetric-stretch peak.

As discussed in section 5.1.1., the reduced splitting in the nitrate peak is believed to result from a small number of water molecules that solvate a single nitrate ion. If true, and if the nitrate ions are solvated in clusters that are composed of 15 to 300 water molecules, the nitrate ions should have a propensity to be located at the exterior of the water clusters, resulting in the nitrate ions having an asymmetric solvation geometry. Interestingly, the area of the high-frequency nitrate peak is larger than the low-frequency nitrate peak, implying that the symmetric nitrate geometry is more abundant in solution. This suggest that the clusters are composed of more than 300 water molecules. If true, the magnitude of the peak splitting of the asymmetric-nitrate peaks should be similar to the splitting in the bulk phase because size of the cluster is representative of the bulk phase. For the nitrate ion that is hydrated by four water molecules, Neumark and coworkers report an experimental peak splitting of 12 cm^{-1}. The smallest calculated peak splitting for a nitrate ion hydrated by four water molecules was 30 cm^{-1}, meaning the arrangement of the water molecules surrounding the nitrate ion that is physically present was unable to be identified. This suggest that the observed peak splitting and peak area ratio in the FTIR spectra may be caused by the hydration of the nitrate ion by four water molecules that are symmetrically arranged around the ion.

It is interesting that more nitrate ions with the symmetric geometry, relative to the nitrate ions with the asymmetric geometry, are found in the clusters compared to the bulk water. Electronic structure calculations of the singly- and doubly-bound nitrate solvation geometries show the doubly-bound geometry is lower in energy than the singly-bound geometry, lending to the belief that the number of doubly-bound nitrate geometries should be larger than the singly-bound in pure water. This peak area ratio in the aqueous KNO_3 cluster spectra raises the question of why more nitrate ions with the asymmetric geometry are present in the bulk phase. To experimentally confirm this theory, the size and composition of these water clusters must be identified.

Comparison of the aqueous KNO_3 cluster spectra that were collected immediately and three weeks after the sample was prepared shows a substantial increase in the area of the high frequency peak in the spectrum that was collected after the sample had aged. The relative increase in the nitrate ions with the symmetric solvation geometry may result from the aggregation of aqueous clusters with time. As the nitrate ion is hydrated by an increasing number of water molecules, the symmetric nitrate geometry becomes energetically stabilized, increasing the relative abundance of the symmetric solvation geometries. If true, the peak splitting is expected to increase because of the increased number of water molecules that hydrate the nitrate ions. Because the peak splitting is unchanged with time, an alternative interpretation that the cations migrate from the CCl_4 into the aqueous clusters could be more accurate. When the samples are sonicated, the potassium ions may partition into the CCl_4.[13] As the clusters are allowed to stabilize with time, the potassium ions are believed to transport into the aqueous KNO_3 clusters. The increased electric fields around the nitrate ion stabilizes the symmetric nitrate ion, as

observed in the bulk phase experiments. Because no attempts have been made to reproduce the change in the peak height areas with time, it is unknown if the change in the areas of the asymmetric-stretch peaks is caused by the stabilization of the symmetric nitrate geometry that may be consistently observed in multiple samples or if this change is an artifact that is unique to the sample.

5.1.3 Unidentified peak

Two additional that are peaks located around 1395 and 1425 cm^{-1} that are not present in the bulk KNO_3 spectra are identified in the aqueous KNO_3 cluster spectra. A similar result was observed in gas phase cluster experiments conducted by Neumark and coworkers.[36] As discussed in section 5.1.2, a shoulder around 1395 cm^{-1} was identified in the IRMPD spectra of the nitrate ion hydrated by four water molecules. This feature is believed to result from the presence of a secondary isomer of the nitrate ion that is hydrated by four water molecules in the gas phase. The same interpretation may be applied to the experimental FTIR spectra. The peaks that are located around 1395 and 1425 cm^{-1} result from an additional nitrate ion isomer that is present in the sample, meaning that two situations are possible. Either additional nitrate solvation geometries (other than the two previously proposed symmetric and asymmetric geometries) exist in the sample or multiple nitrate ion isomers exist in the sample that causes the vibrational frequencies of the nitrate asymmetric stretches to be red shifted. Because these two additional peaks have not been observed in the spectra of other aqueous KNO_3 cluster samples, the possibility that these peaks may be an artifact that is unique to the sample for which the two additional peaks are present is deemed to be more likely than the latter explanations. If these peaks are an

artifact of the sample, they may be caused by the inability to consistently introduce the same amount of water into the samples at this time.

5.2 Hydrogen Bonding Effects to Infrared Windows

In recent years, multiple studies have used aqueous clusters of ions that are dispersed in CCl_4 to investigate the formation of water clusters and pure solvent effects on the solvation structure of an ion.[43,60,61] Discrepancies among the spectra of aqueous solutions have arisen due to the reported presence or absence of H-bonding in the systems that have been studied.[43] Shultz and coworkers assert that these disagreements result from the H-bonding of water molecules to the IR cell windows. To prevent the aqueous KNO_3 clusters from H-bonding to the long-path cell or the CaF_2 windows that are used to collect the FTIR spectra of the samples, the cell was silanized and attempts were made to silanize the CaF_2 windows. Hydrophobicity of the windows was qualitatively determined by contact angle of a drop of water on the window. Comparing the contact angle before and after the CaF_2 window underwent the silanziation process, the hydrophobicity of the windows was deemed to decrease. All attempts increased the CaF_2 affinity for water, including attempts in which a glass microscope slide (which was used as an indicator for the successful creation of the silanol solution) and a CaF_2 window underwent the same silanzation process with the same silanol solution.

Because of the failed attempts to silanize the CaF_2 windows, germanium windows, which are hydrophobic, were used. These windows were chosen rather than following a silanization process that is meant for CaF_2 materials because of the difficulty and cost of this alternative procedure.[62] Before spectra of the aqueous KNO_3 cluster samples were collected, a background of the long-path cell that was fitted with germanium windows and

filled with dry nitrogen gas was collected. To ensure the background of the long-path cell was correctly obtained, a spectrum (Figure 5.2) of the empty cell, still filled with nitrogen gas, was collected immediately after the background spectrum was collected.

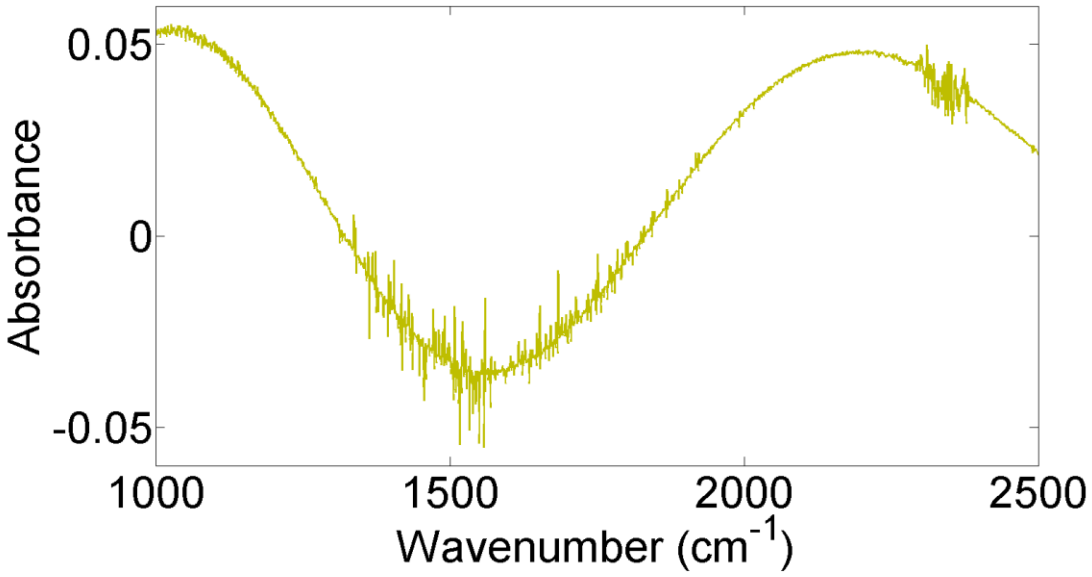

Figure 5.2. FTIR spectrum of the long-path cell fitted with Ge windows.

The spectrum of the empty sample cell shows a nonzero and nonlinear lineshape inside and outside of the region that the nitrate asymmetric-stretch peak is located. The long wavelength of the lineshape suggest that the IR light that passes through the long-path cell is reflected off the surfaces of each window. The absence of the lineshape in the FTIR spectrum of a single Ge window confirms the lineshape in Figure 5.2 is caused by the etalon effect. Fabrication of an apparatus to angle the long path cell so the Ge windows are not orthogonal to the incident IR radiation would eliminate this effect.

5.3 Replacement Solvents for Carbon Tetrachloride

Following the procedures of Shultz and coworkers, CCl_4 was used as the solvent in this

experiment because of the low solubility of water in the solvent.[43] Moreover, as shown in Figure 5.3, CCl_4 does not strongly absorb IR light in the region that the nitrate asymmetric-stretch peak is located, allowing the nitrate peak to be identified. Similar to what was observed with the water spectrum in the bulk nitrate experiments, the CCl_4 absorption bands that are located directly above and below the asymmetric-stretch nitrate peak may influence the lineshape of the nitrate peak. Other solvents in which water has a low solubility and does not strongly absorb IR light in or near the region of the asymmetric-stretch nitrate peak, which may cause the nitrate peak to be altered, were investigated.

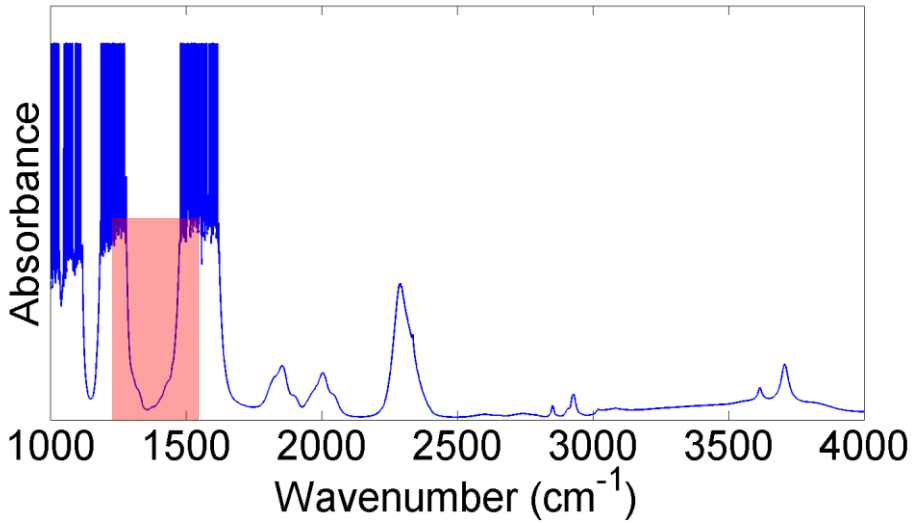

Figure 5.3. FTIR spectrum of CCl_4. The region of the nitrate asymmetric-stretch is indicated by the shaded box.

To limit the financial cost of searching for replacement solvents, IR spectra of the potential solvents in Figure 5.4 were calculated. Solvents were chosen by identifying symmetric molecules that are commonly used in IR spectroscopy experiments, such as cyclohexane and CCl_4. The requirement that the molecules must be symmetric eliminates polar molecules so that nitrate and water will not be soluble in the solvent. Derivatives of

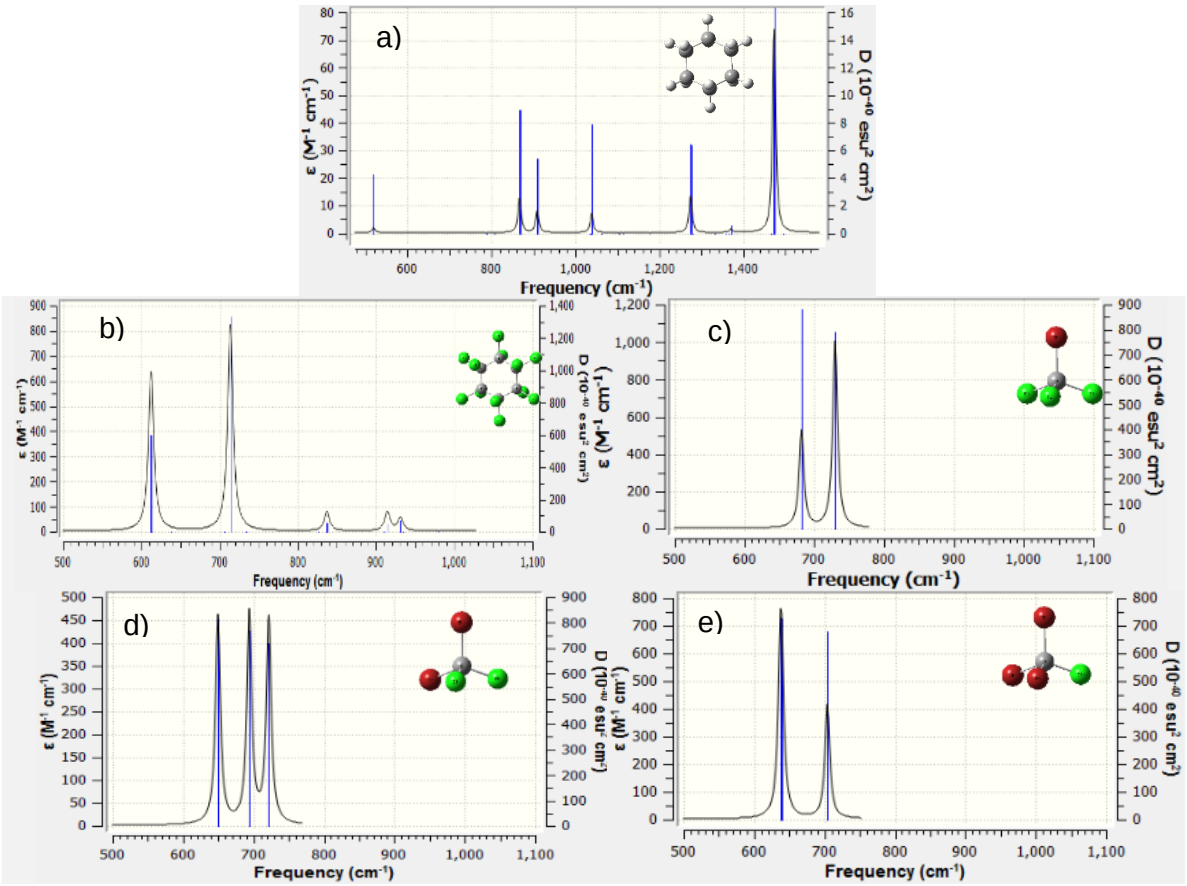

Figure 5.4. B3LYP/aug-cc-PVDZ calculated IR spectra of cyclohexane (a), dodecachlorocyclohexzne (b), bromotrichloromethane (c), dibromodichloromethane (d), tribromochloromethane (e).

CCl_4 that substituted chlorine atoms with bromine atoms (dodecachlorocyclohexane, bromotrichloromethane, dibromodichloromethane, and tribromochloromethane) were also tested. Replacing chlorine atoms with bromine atoms dampens or increases the vibrational frequencies of the molecule, causing the peaks in the IR spectrum to be red- or blue-shifted. Testing these different solvents allows for the shifts in the spectrum to be visualized so it can be determined if the region in the IR spectrum that the nitrate asymmetric-stretch peak is located becomes clear. B3LYP/aug-cc-PVDZ calculated spectra for each molecule are presented in Figure 5.4. Of the possible replacement solvents, all except cyclohexane do

not have absorbance peaks that are located in the region that the nitrate asymmetric-stretch peak is found, indicating that the molecules (other than cyclohexane) are reasonable replacements for CCl_4. Calculations for dodecabromocyclohexane were attempted, but did not converge. Because the peaks in the calculated dodecachlorocyclohexane spectrum are displaced far away from the region where the nitrate asymmetric-stretch peaks are located, the shifts in the IR peaks that are caused by substituting the chlorine atoms with bromine atoms should not interfere with the nitrate peak, making it a suitable replacement for CCl_4. Once all of the calculations were completed, the cost and availability of the reagents were checked. Because of the high price of these solvents or because they are commercially unavailable, it is unreasonable for these reagents to be used in the experiment until these methods are perfected.

5.4 Conclusions

Evidence suggest that water energetically stabilizes the symmetric nitrate solvation geometry. The increase in the peak area ratio with time, which suggests that the relative abundance of the symmetric solvation geometry increases with time, is believed to result from the migration of the potassium ions from the CCl_4 into the aqueous KNO_3 clusters. If the peak splitting increased with time, the aggregation of water clusters is believed to change the ratio of the peak areas. As the strength of the electric fields that surround the nitrate ion increases, the relative abundance of the symmetric nitrate geometry increases, as observed in the bulk phase experiments.

Insight into the stability of the two nitrate solvation geometries in water clusters may elucidate changes in the composition of nitrate-containing aerosols. MD simulations that were performed by Gerber and coworkers showed that a nitrate ion that is solvated in a

cluster of 15 to 300 water molecules is located at the exterior while the nitrate ion is solvated in the interior of clusters that contain more than 300 water molecules. Results from these experiments may provide evidence for the location of the nitrate ion in aqueous aerosols particles that are composed of a varying number of water molecules. This information may be used to help predict compositional changes of the particle with time.[59]

To understand the effects that varying sizes of water clusters have on the relative stability of the nitrate solvation geometries, the number of water molecules that hydrate each nitrate ion needs to be determined. The potential for water cluster to H-bond to the surface of CaF_2 windows, which could cause the water clusters to aggregate at the window surface, needs to be minimized by using Ge window to which water clusters will not H-bond. MD simulations that attempt to replicate the size of the aqueous clusters and identify the location of the potassium ions in the samples are underway. Completion of these simulations may help interpret the changes that are observed in the experimental spectra of the aqueous KNO_3 clusters. The influence that the water molecules and ionic strength have on the relative abundance of the two solvation geometries may be achieved by replicating bulk phase experiments for nitrate concentrations that are experienced in the cluster experiments. With the nitrate ions exposed to an ionic strength that is equivalent to what is observed in the aqueous clusters, but solvated by a larger number of water molecules that is found in the bulk phase, the changes in the aqueous KNO_3 cluster spectra can be identified to result from the reduced number of hydrating water molecules or from the reduced ionic strength in the sample. Furthermore, the collection of temperature-dependent spectra would allow the relative difference in energy between the two solvation geometries

in a limited water environment to be determined. Results from this experiment may help explain the increase in area of the high frequency peak as the sample aged.

6. Conclusions

Understanding the photolysis of the nitrate ion on a molecular level may be helpful in modeling atmospheric conditions. To increase the ability of such models to reproduce the physical conditions of the atmosphere, the identity and quantity of the compounds that are present in this medium must be known. This requires a molecular understanding of the factors that influence the production of atmospheric gases, which is especially important for chemically complex mediums such as snowpack and aerosol particles. Both media are composed of multiple compounds that influence the product ratio of the photolysis of the nitrate ion in ways that are unknown. Therefore, it is difficult to predict the branching ratio of the products from the photolysis of the nitrate ion. Understanding the effects that less chemically complex environments have on the photochemistry of the nitrate ion allows a more comprehensive understanding of how the composition of these different mediums influence the product ratio of the products of the photolysis of the nitrate ion can be obtained. To completely understand how different factors influence the photochemistry of the nitrate ion, the effect that pure water has on the stability of the solvation geometries of the nitrate ion was investigated. FTIR spectra suggest that the symmetric nitrate geometry is energetically favored compared to the asymmetric geometry. This is consistent with electronic structure calculations of the nitrate ion that is hydrated by a single water, which shows that the symmetric geometry is energetically favored compared to the asymmetric geometry. This apparent increased favorability for the symmetric nitrate geometry that is solvated in a water cluster raises questions about why the relative amount of the asymmetric nitrate geometry is larger compared to the symmetric nitrate geometry in the

bulk aqueous KNO_3 solutions. This may result from the stabilization of the asymmetric nitrate geometry in bulk water.

Changes in the relative ratio of the nitrate ion solvation geometries may have implications with the ratio of products that are produced from the photolysis of the nitrate ion. Grassian and coworkers showed that the amount of nitrite that is produced from the photolysis of sodium nitrate is dependent on the nitrate concentration in solution.[3] This increased production of nitrite is caused by an increase in the number of nitrate ions that photodissociate through pathway 2 of Table 1.1. Experiments that are presented in Chapter 3 show that the area of the high frequency asymmetric-stretch feature in the KNO_3 is proportional to the ionic strength of the solution, suggesting that the initial reaction pathway that is taken during the photolysis of the nitrate ion is correspondent of the symmetric nitrate geometry. Although this observation does not definitively prove that the initial reaction pathway that is taken during photolysis is dependent on the solvation geometry, it does suggest that there is some relationship between the solvation geometry and the pathway, which may explain the ionic strength dependence.

The experiments that are presented here support, but are unable to definitively confirm, the existence of two nitrate and two carbonate ion solvation geometries in solution because the structures of the geometries cannot be determined. Assuming that two solvation geometries exist in solution, evidence suggests that the relative ratio of the two geometries is dependent on the ionic concentration in the solution. This dependence is believed to result from the stabilization of one geometry with increases in electric field strengths in solution. Interestingly, the relative areas of the two asymmetric-stretch features in the KNO_3 and K_2CO_3 spectra are inversely proportional with ionic strength: the relative area

of the low frequency asymmetric-stretch feature of the KNO_3 spectrum decreases with ionic concentration while the relative area of the high frequency asymmetric-stretch feature of K_2CO_3 increases with ionic concentration. Based upon electronic structure calculations for the singly- and doubly-bound solvation geometries, it is reasonable to assume that the low frequency stretch feature in the K_2CO_3 FTIR spectrum results from the asymmetric carbonate geometry while the high frequency feature results from the symmetric carbonate geometry. Unlike for the nitrate ion, a global minimum energy structure for the singly-bound geometry is unable to be found for the carbonate ion, unless the SMD is used. Therefore, it is currently unknown which carbonate solvation geometry (symmetric or asymmetric) is associated with the high and low frequency asymmetric-stretching features in the K_2CO_3 IR spectrum. If the low frequency feature results from the symmetric geometry, the hypothesis that strong electric fields stabilize the symmetric solvation structures is supported. If the low frequency feature results from the asymmetric geometry, an alternative factor may cause the nitrate and carbonate solvation geometries to be stabilized. To identify the reason for the stabilization of the nitrate and carbonate ion geometries, a secondary structure for the carbonate ion that is hydrated by a single water molecule needs to be found.

Changes in the relative ratio of the carbonate ion solvation geometries in the bulk phase may help identify the location of the carbonate ion in aerosol particles. As discussed in Chapter 5, the location of the nitrate ion in water clusters may be used to determine the location of the ion in an aerosol particle. The same may be done for the carbonate ion. Before the aqueous K_2CO_3 clusters that are dispersed in CCl_4 can be probed, how the carbonate ion behaves in the bulk phase needs to be first understood. Once a molecular

understanding of how the two carbonate solvation geometries respond to changes to temperature and ionic concentration in the bulk solution is achieved, the geometries of the carbonate ions that are solvated water clusters with unknown sizes and compositions can start to be understood.

Evidence supports the existence of two solvation geometries of nitrate and carbonate ions in solution. Because the experiments that are presented here are unable to identify the exact structures of the two solvation geometries, the existence of two different structures cannot be definitively confirmed. The presence of two additional peaks in the aqueous KNO_3 cluster spectra brings into question the accuracy of the two structure model; more than two solvation geometries may exist in solution. It is possible that the two peaks result from solvation geometries other than the specific types of geometries that have been proposed by electronic structure calculations. Because these two peaks have not been observed in the bulk-aqueous KNO_3 FTIR spectra, the existence of these two additional peaks weakly suggest that additional solvation geometries exist in solution. If the two additional peaks are caused by the presence of additional classes of solvation geometries in solution, it is reasonable to expect the two peaks to be present in the bulk phase FTIR spectra. Compared to the aqueous KNO_3 clusters, there are significantly more nitrate ions in the bulk-aqueous KNO_3 samples. If more than two solvation geometries exist, the number of nitrate ions with the unidentified solvation geometries is expected to be larger in the bulk phase because there are more nitrate ions that can experience the additional solvation geometries. Even though the additional peaks have not been observed in other KNO_3 spectra, the inability to identify the source of the additional peaks at this time prevents the possibility that more than two solvation geometries exist in solution to be

dismissed. Multiple geometries may be present in the clusters. A more extensive search for a minimum energy structure for the carbonate ion that is hydrated by a single water molecule is required to determine if more than two solvation geometries are present in solution.

7. Bibliography

1. Mason, P. E.; Wernersson, E.; Jungwirth, P. Accurate Description of Aqueous Carbonate Ions: An Effective Polarization Model Verified by Neutron Scattering. *J. Phys. Chem. B.* **2012**, 116 (28), 8145.

2. Vchirawongkwin, V.; Sato, H.; Sakaki, S. RISM-SCF-SEDD Study on the Symmetry Breaking of Carbonate and Nitrate Anions in Aqueous Solution. *J. Phys. Chem. B* **2010**, *114* (32), 10513.

3. Roca, M.; Zahardis, J.; Bone, J.; El-Maazawi, M.; Grassian, V. H. 310 nm Irradiation of Atmospherically Relevant Concentrated Aqueous Nitrate Solutions: Nitrite Production and Quantum Yields. *J. Phys. Chem. A* **2008**, *112* (51), 13275.

4. Wang, Z.-H.; Miao, Y.-F.; Li, S.-X. Effect of Ammonium and Nitrate Nitrogen Fertilizers on Wheat Yield in Relation to Accumulated Nitrate at Different Depths of Soil in Drylands of China. *Field Crops Res.* **2015**, *183 (1)*, 211.

5. Gibson, E. R.; Hudson, P. K.; Grassian, V. H. Aerosol Chemistry and Climate: Laboratory Studies of the Carbonate Component of Mineral Dust and its Reaction Products. *Geophys. Res. Lett.* **2006**, *33* (13), L13811.

6. Hudson, P. K.; Schwarz, J.; Baltrusaitis, J.; Gibson, E. R.; Grassian, V. H. A Spectroscopic Study of Atmospherically Relevant Concentrated Aqueous Nitrate Solutions. *J. Phys. Chem. A* **2007**, *111* (4), 544.

7. Honrath, R. E.; Peterson, M. C.; Guo, S.; Dibb, J. E.; Shepson, P. B.; Campbell, B. Evidence of NO_x Production within or upon Ice Particles in the Greenland Snowpack. *Geophys. Res. Lett.* **1999**, *26* (6), 695.

8. Hallquist, M.; Wenger, J. C.; Baltensperger, U.; Rudich, Y.; Simpson, D.; Claeys,

M.; Dommen, J.; Donahue, N. M.; George, C.; Goldstein, A. H.; et al. The Formation, Properties and Impact of Secondary Organic Aerosol: Current and Emerging Issues. *Atmos. Chem. Phys.* **2009**, *9* (14), 5155.

9. Valley, N. A.; Richmond, G. L. Computational Vibrational Sum Frequency Spectra of Formaldehyde and Hydroxymethanesulfonate at Aqueous Interfaces. *J. Phys. Chem. C* **2016**, *120* (26), 14122.

10. Plath, K. L.; Valley, N. A.; Richmond, G. L. Ion-Induced Reorientation and Distribution of Pentanone in the Air–Water Boundary Layer. *J. Phys. Chem. A* **2013**, *117* (45), 11514.

11. Otten, D. E.; Petersen, P. B.; Saykally, R. J. Observation of Nitrate Ions at the Air/Water Interface by UV-Second Harmonic Generation. *Chem. Phys. Lett.* **2007**, *449* (4–6), 261.

12. Xu, M.; Spinney, R.; Allen, H. C. Water Structure at the Air−Aqueous Interface of Divalent Cation and Nitrate Solutions. *J. Phys. Chem. B* **2009**, *113* (13), 4102.

13. Bisson, P.; Xiao, H.; Kuo, M.; Kamelamela, N.; Shultz, M. J. Ions and Hydrogen Bonding in a Hydrophobic Environment: CCl_4. *J. Phys. Chem. A* **2010**, *114* (12), 4051.

14. Domine, F.; Bock, J.; Voisin, D.; Donaldson, D. J. Can We Model Snow Photochemistry? Problems with the Current Approaches. *J. Phys. Chem. A* **2013**, *117* (23), 4733.

15. Traversi, R.; Udisti, R.; Frosini, D.; Becagli, S.; Ciardini, V.; Funke, B.; Lanconelli, C.; Petkov, B.; Scarchilli, C.; Severi, M.; et al. Insights on Nitrate Sources at Dome C (East Antarctic Plateau) from Multi-Year Aerosol and Snow Records. *Tellus B* **2014**, *66* (1), 22550.

16. Bock, J.; Savarino, J.; Picard, G. Air–snow Exchange of Nitrate: A Modelling Approach to Investigate Physicochemical Processes in Surface Snow at Dome C, Antarctica. *Atmos. Chem. Phys.* **2016**, *16* (19), 12531.

17. Fibiger, D. L.; Hastings, M. G.; Dibb, J. E.; Huey, L. G. The Preservation of Atmospheric Nitrate in Snow at Summit, Greenland. *Geophys. Res. Lett.* **2013**, *40* (13), 3484.

18. Geng, L.; Cole-Dai, J.; Alexander, B.; Erbland, J.; Savarino, J.; Schauer, A. J.; Steig, E. J.; Lin, P.; Fu, Q.; Zatko, M. C. On the Origin of the Occasional Spring Nitrate Peak in Greenland Snow. *Atmos. Chem. Phys.* **2014**, *14* (24), 13361.

19. Meusinger, C.; Berhanu, T. A.; Erbland, J.; Savarino, J.; Matthew S. Laboratory Study of Nitrate Photolysis in Antarctic Snow. I. Observed Quantum Yield, Domain of Photolysis, and Secondary Chemistry. *J. Chem. Phys.* **2014**, *140* (24), 244305.

20. Björkman, M. P.; Vega, C. P.; Kühnel, R.; Spataro, F.; Ianniello, A.; Esposito, G.; Kaiser, J.; Marca, A.; Hodson, A.; Isaksson, E.; et al. Nitrate Postdeposition Processes in Svalbard Surface Snow: NO_3^- Post-Deposition Processes, Svalbard. *J. Geophys. Res. Atmos.* **2014**, *119* (22), 12953.

21. Duderstadt, K. A.; Dibb, J. E.; Schwadron, N. A.; Spence, H. E.; Solomon, S. C.; Yudin, V. A.; Jackman, C. H.; Randall, C. E. Nitrate Ion Spikes in Ice Cores Not Suitable as Proxies for Solar Proton Events. *J. Geophys. Res. Atmos.* **2016**, 121 (6), 2994.

22. Bock, J.; Jacobi, H.-W. Development of a Mechanism for Nitrate Photochemistry in Snow. *J. Phys. Chem. A* **2010**, *114* (4), 1790.

23. Thøgersen, J.; Gadegaard, A.; Nielsen, J.; Jensen, S. K.; Petersen, C.; Keiding, S. R. Primary Formation Dynamics of Peroxynitrite Following Photolysis of Nitrate. *J.*

Phys. Chem. A **2009**, *113* (39), 10488.

24. Dubowski, Y.; Colussi, A. J.; Hoffmann, M. R. Nitrogen Dioxide Release in the 302 nm Band Photolysis of Spray-Frozen Aqueous Nitrate Solutions. Atmospheric Implications. *J. Phys. Chem. A* **2001**, *105* (20), 4928.

25. Jacobi, H.-W.; Hilker, B. A Mechanism for the Photochemical Transformation of Nitrate in Snow. *J. Photochem. Photobiol. Chem.* **2007**, *185* (2–3), 371.

26. Cheung, J. L.; Li, Y. Q.; Boniface, J.; Shi, Q.; Davidovits, P.; Worsnop, D. R.; Jayne, J. T.; Kolb, C. E. Heterogeneous Interactions of NO_2 with Aqueous Surfaces. *J. Phys. Chem. A* **2000**, *104* (12), 2655.

27. Mack, J.; Bolton, J. R. Photochemistry of Nitrite and Nitrate in Aqueous Solution: A Review. *J. Photochem. Photobiol. Chem.* **1999**, *128* (1–3), 1.

28. Hoigné, J.; Bader, H. Rate Constants of Reactions of Ozone with Organic and Inorganic Compounds in Water—I. *Water Res.* **1983**, *17* (2), 173.

29. Jacobi, H.-W.; Annor, T.; Quansah, E. Investigation of the Photochemical Decomposition of Nitrate, Hydrogen Peroxide, and Formaldehyde in Artificial Snow. *J.*

30. Chu, L.; Anastasio, C. Formation of Hydroxyl Radical from the Photolysis of Frozen Hydrogen Peroxide. *J. Phys. Chem. A* **2005**, *109* (28), 6264.

31. Christensen, H.; Sehested, K.; Corfitzen, H. Reactions of Hydroxyl Radicals with Hydrogen Peroxide at Ambient and Elevated Temperatures. *J. Phys. Chem.* **1982**, *86* (9), 1588.

32. Bielski, B. H. J.; Cabelli, D. E.; Arudi, R. L.; Ross, A. B. Reactivity of HO_2/O^-_2 Radicals in Aqueous Solution. *J. Phys. Chem. Ref. Data* **1985**, *14* (4), 1041.

33. Christensen, H.; Sehested, K. Hydroperoxo and Oxygen (1-) Radicals at Elevated

Temperatures. *J. Phys. Chem.* **1988**, *92* (10), 3007.

34. Elliot, A. J.; Buxton, G. V. Temperature Dependence of the Reactions OH + O^-_2 and OH + HO_2 in Water up to 200 °C. *J. Chem. Soc., Faraday Trans.* **1992**, *88* (17), 2465.

35. Herrmann, H.; Ervens, B.; Nowacki, P.; Wolke, R.; Zellner, R. A Chemical Aqueous Phase Radical Mechanism for Tropospheric Chemistry. *Chemosphere* **1999**, *38* (6), 1223.

36. Goebbert, D. J.; Garand, E.; Wende, T.; Bergmann, R.; Meijer, G.; Asmis, K. R.; Neumark, D. M. Infrared Spectroscopy of the Microhydrated Nitrate Ions NO_3^- $(H_2O)_{1–6}$. *J. Phys. Chem. A* **2009**, *113* (26), 7584.

37. Wang, X.-B.; Yang, X.; Wang, L.-S.; Nicholas, J. B. Photodetachment and Theoretical Study of Free and Water-Solvated Nitrate Anions, $NO_3^-(H_2O)_n$ (n=0–6). *J. Chem. Phys.* **2001**, *116* (2), 561.

38. Shen, M.; Xie, Y.; Schaefer, H. F.; Deakyne, C. A. Hydrogen Bonding between the Nitrate Anion (Conventional and Peroxy Forms) and the Water Molecule. *J. Chem. Phys.* **1990**, *93* (5), 3379.

39. Pathak, A. K.; Mukherjee, T.; Maity, D. K. Microhydration of NO_3^-: A Theoretical Study on Structure, Stability and IR Spectra. *J. Phys. Chem. A* **2008**, *112* (15), 3399.

40. Simeon, V.; Butorac, V.; Tomišić, V.; Kallay, N. Existence of Two Forms of Nitrate Ion in Dilute Aqueous Solutions. Thermodynamic Parameters of Interconversion. *Phys. Chem. Chem. Phys.* **2003**, *5* (10), 2015.

41. Goss, L. M.; Sharpe, S. W.; Blake, T. A.; Vaida, V.; Brault, J. W. Direct Absorption Spectroscopy of Water Clusters. *J. Phys. Chem. A* **1999**, *103* (43), 8620.

42. Wende, T. Gas Phase Infrared Photodissociation Spectroscopy of Mass-Selected Ionic Clusters: Metal Oxides and Microhydrated Anions. Ph.D. Dissertation, Freie Universität, Berlin, Berlin, 2012.

43. Kuo, M. H.; David, A.; Kamelamela, N.; White, M.; Shultz, M. J. Nitric Acid-Water Interaction Probed via Isolation in Carbon Tetrachloride. *J. Phys. Chem. C* **2007**, *111* (25), 8827.

44. Frisch, M. J.; Trucks, G. W.; Schlegel, H. B.; Scuseria, G. E.; Robb, M. A.; Cheeseman, J. R.; Scalmani, G.; Barone, V.; Mennucci, B.; Petersson, G. A. *Gaussian 09*, Revision B.01, Gaussian: Wallingford CT, 2009.

45. Becke, A. D. Density-Functional Thermochemistry. III. The Role of Exact Exchange. *J. Chem. Phys.* **1993**, *98* (7), 5648.

46. Dunning, T. H., Jr. Gaussian Basis Sets for Use in Correlated Molecular Calculations. I. The Atoms Boron through Neon and Hydrogen. *J. Chem. Phys.* **1989**, *90* (2), 1007.

47. Bergonzi, I.; Mercury, L.; Brubach, J.-B.; Roy, P. Gibbs Free Energy of Liquid Water Derived from Infrared Measurements. *Phys. Chem. Chem. Phys.* **2014**, *16* (45), 24830.

48. Geissler, P. L. Temperature Dependence of Inhomogeneous Broadening: On the Meaning of Isosbestic Points. *J. Am. Chem. Soc.* **2005**, *127* (42), 14930.

49. Jones, K. K.; Eckler, L. H.; Nee, M. J. Effect of Ionic Strength on Solvation Geometries in Aqueous Nitrate Ion Solutions. *J. Phys. Chem. A* **2017**, *121* (12), 2322.

50. Laskin, A.; Iedema, M. J.; Ichkovich, A.; Graber, E. R.; Taraniuk, I.; Rudich, Y. Direct Observation of Completely Processed Calcium Carbonate Dust Particles. *Faraday*

Discuss. **2005**, *130 (1)*, 453.

51. Vchirawongkwin, V.; Kritayakornupong, C.; Tongraar, A.; Rode, B. M. Symmetry Breaking and Hydration Structure of Carbonate and Nitrate in Aqueous Solutions: A Study by Ab Initio Quantum Mechanical Charge Field Molecular Dynamics. *J. Phys. Chem. B* **2011**, *115* (43), 12527.

52. Fournier, J. A.; Carpenter, W.; De Marco, L.; Tokmakoff, A. Interplay of Ion–Water and Water–Water Interactions within the Hydration Shells of Nitrate and Carbonate Directly Probed with 2D IR Spectroscopy. *J. Am. Chem. Soc.* **2016**, *138* (30), 9634.

53. NIST Computational Chemistry Comparison and Benchmark Database NIST Standard Reference Database Number 101 Release 19, April 2018, Editor: Russell D. Johnson III

54. MATLAB, Version 8.1.0.604 *(R2013a)*, The MathWorks, Inc. Natick, MA 2013

55. Pathak, A. K.; Mukherjee, T.; Maity, D. K. IR Spectra of Carbonate-Water Clusters, $CO_3^-(H_2O)_n$: A Theoretical Study. *Synth. React. Inorg. Met.-Org. Nano-Met. Chem.* ***2008***, *38* (1), 76.

56. Pathak, A. K.; Maity, D. K. Distinctive IR Signature of $CO_3^{\bullet-}$ and CO_3^{2-} Hydrated Clusters: A Theoretical Study. *J. Phys. Chem. A* **2009**, *113* (48), 13443.

57. Marenich, A. V.; Cramer, C. J.; Truhlar, D. G. Universal Solvation Model Based on Solute Electron Density and on a Continuum Model of the Solvent Defined by the Bulk Dielectric Constant and Atomic Surface Tensions. *J. Phys. Chem. B* **2009**, *113* (18), 6378.

58. Xiang, T.; Anderson, B. D. Conformational Structure, Dynamics, and Solvation

Energies of Small Alanine Peptides in Water and Carbon Tetrachloride. *J. Pharm. Sci.* **2006**, *95* (6), 1269.

59. Miller, Y.; Thomas, J. L.; Kemp, D. D.; Finlayson-Pitts, B. J.; Gordon, M. S.; Tobias, D. J.; Gerber, R. B. Structure of Large Nitrate−Water Clusters at Ambient Temperatures: Simulations with Effective Fragment Potentials and Force Fields with Implications for Atmospheric Chemistry. *J. Phys. Chem. A* **2009**, *113* (46), 12805.

60. Danten, Y.; Tassaing, T.; Besnard, M. Molecular Dynamics of Monomeric Water Dissolved in Very Hydrophobic Solvents: The Current State of the Art of Vibrational Spectroscopy Analyzed from Analytical Model and MD Simulations. *J. Phys. Chem. A* **2000**, *104* (42), 9415.

61. Köddermann, T.; Schulte, F.; Huelsekopf, M.; Ludwig, R. Formation of Water Clusters in a Hydrophobic Solvent. *Angew. Chem. Int. Ed.* **2003**, *42* (40), 4904.

62. Padermshoke, A.; Konishi, S.; Ara, M.; Tada, H.; Ishibashi, T.-A. Novel SiO_2 Deposited CaF_2 Substrate for Vibrational Sum-Frequency Generation (SFG) Measurements of Chemisorbed Monolayers in an Aqueous Environment. *Appl. Spectrosc.* **2012**, *66* (6), 711.

.